DESIGN, SYNTHESIS, AND BIOLOGICAL ACTIVITY PROFILING STUDY OF IMIDAZOLINONE-BASED HYDRAZONES AS POTENTIAL MULTITARGET ANTIMYCOBACTERIAL AGENTS

Enas A. Taha[1*], Nadia M. Mahfouz[1,2], Farghaly A. Omar[2], Yasser Musa Ibrahim[3] and Ahmed Megahed Abouwarda[3]

[1]*Chemistry Deptertment, Faculty of Pharmacy, October 6 University, 6 October City 12585, Giza/ Egypt*
[2]*Medicinal Chemistry Deptertment, Faculty of Pharmacy, Assiut University, Assiut 71526 Egypt*
[3]*Microbiology Deptertment, General Division of Basic Medical Sciences, Egyptian Drug Authority (EDA), Giza 12611, Egypt*

*The current investigation involves design, synthesis, and assessment of the potential antimycobacterial activity of three sets of 4,4-diphenylimidazolidinone-2-hydrazone derivatives, **3a-l**, **4a-h**, and **5a,b**. Their In vitro efficacy against M. smegmatis ATCC 607 was assessed versus isoniazid (INH) as reference drug. The results revealed that, ten of the tested compounds exhibited inhibitory ability analogous to INH, with MIC values ranging from 0.032 to 0.45 µM (INH: 0.046 µM). Explicitly, the p-tolylethylidene hydrazone **4c** and the 2-oxoindoline-3-ylidene **5a** are the most potent compounds (MIC = 0.033 µM). Compound **5a** exhibited bactericidal effect equivalent to INH, as evidenced by the time-kill kinetics pattern (≥ 3 log reduction in bacterial count: 99.9 % killing), at 4x MIC value, after 72 h of incubation. Cytotoxicity assessment of the most potent compounds, **4a,c,e, 5a,b,** against Vero cells line, revealed minimal in vitro cytotoxicity (SI ~ 40 - > 2000). Bioactivity profiling analysis using several computational and inverse molecular modeling approaches revealed that the studied compounds exhibit multitarget potential as antimycobacterials. The results indicate that mycobacterial acyl-carrier-protein reductase (InhA) is the most credible potential target. Molecular docking studies in the active site of ACP reductase (InhA) revealed promising interaction with the catalytic triad amino acid residues, Tyr 158, Lys165, and phe149. Computational assessment of the molecular characteristics and drug-like scores demonstrate prospective eligibility for further assessments as new series of antimycobacterial agents. The attained results suggest that the studied arylidene hydrazinylimidazolidinones be worthy for further optimization for antimycobacterial activity*

Key words: *Imidazolinone; Hydrazones; Antimycobacterial activity; Cytotoxicity; Bioactivity Profiling; Molecular Modeling*

INTRODUCTION

Tuberculosis infection (TB) is a contagious disease resulting from a unique bacterial strain. The disease regarded as one of the higher causes of death worldwide. It is established globally that there are three main types of mycobacterial infections: the most common form is the drug-susceptible (DS-TB)[1], however, the two others are the multidrug-resistant (MDR-TB), and extensively drug-resistant (XDR-TB)[2]. The greatest barrier to eradication and/or successful control of TB is the emergence of drug-resistant strains of TB[3]. Moreover, long-term therapeutic regimen, patient non-compliance remains the most important reason for treatment failure. This situation brings increased urgency to the task of developing efficacious

antimycobacterial compounds based on novel chemical scaffolds.

One of the fruitful approaches devoted to mycobacterial chemotherapy is the efforts placed on investigating mycobacterial cell envelope structure and the biosynthesis of its hallmark entities to identify attractive drug targets[4]. Several drugs were acknowledged, targeting the biosynthesis of mycolic acids, e.g. isoniazid, ethionamide, thiocarlide, thiacetazone[5-8]. In addition, novel antitubercular drugs such as Delamanid and Bedaquiline, targeting alternative mycobacterial cellular biosynthesis machinery, were also approved [9,10]. Meanwhile, different scaffolds were identified including indole-2-carboxamides I[11,12], phenoxyphenol derivatives II[13], pyrrolidone carboxamides III[14], thiadiazolylhydrazones IV[15], and diphenylpyrazole carboxamides V[16,17], (Fig. 1). The results of these hits highlight their therapeutic potential in treatment of mycobacterial infections and motivate development of new chemical entities. Unfortunately, clinical approval of most of the above drug candidates has been hampered by several difficulties involving limited pharmacokinetic characteristics, severe side effects, resistance development through genetic mutations and/or enhanced efflux of the drugs[18].

Compounds compressing hydrazide-hydrazone motif are reported to display significant anti-TB activity [19-21], in addition to activities against further infectious diseases such as bacterial infections and malaria [22,23]. Evidently, the observed antimicrobial activities are attributed to the ability of these structural functionalities to interfere with vital biochemical processes of respective infectious agents.

Imidazoles are important heterocycles that exists in the core structure of many drugs and lead compounds for combating infectious diseases. Interestingly, disubstituted imidazole derivatives were reported to be potential antimycobacterial bacterial agents functioning as inhibitors of enoyl acyl carrier protein reductase (FabI)[24]. This provided a good incentive to develop novel structures that could be endowed with less toxic features and better activity.

Accordingly, it is anticipated to design and synthesis a series of 2-(aryl/hetroaryl-hydrazono)-4,4-diphenylimidazolinones (Fig. 2) to be tested for their potential antimycobacterial activity. The design strategy involves pharmacophoric features comprising diphenylimidazolinone scaffold as 5-membered heterocyclic isostere to the above-mentioned lead compounds. The diphenyl-substituent imparts lipophilic trait, which likely enhances the permeability of the molecules into the lipophilic inner membrane of mycobacterium. The two N-atoms and the C=O allow H-bonding elements in the interaction with the target protein. Additionally, the pendant arylhydrazone moiety might be involved in the redox aspects of the target enzymes. Moreover, adding substituents, with variable physicochemical characteristics, to the terminal aryl moieties might manipulate the potential activity of the designed compounds. Ultimately, computational assessment of activity profiling to elucidate the possible mechanism of action of the synthesized compounds. Moreover, cytotoxicity study and drug-likeness characteristics will also be discussed.
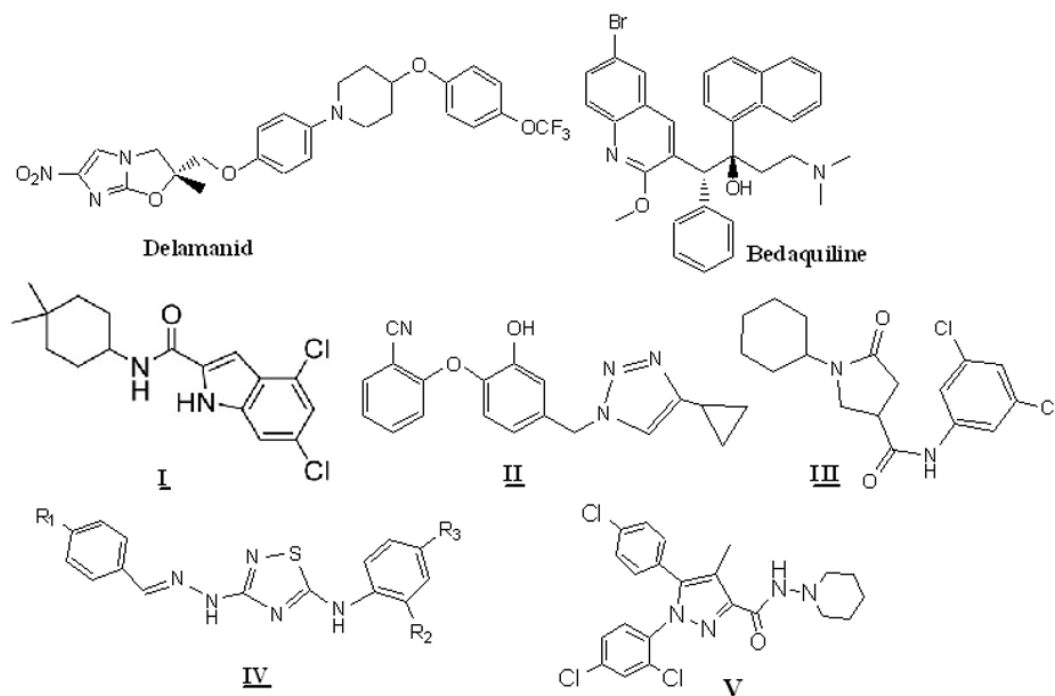
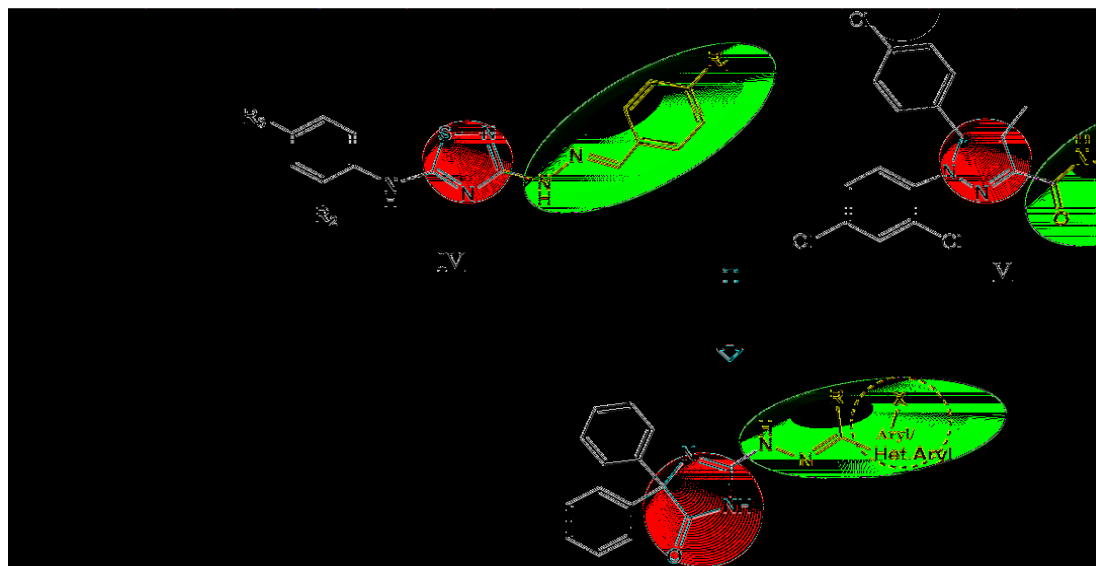**Fig. 1:** Representative examples of approved antitubercular drugs and some reported lead compounds.

Fig. 2: Design strategy of 2-(aryl/hetroarylhydrazono)-4,4-diphenyl-imidazolinones.

RESULTS AND DISCUSSION

Results
Chemistry

The synthesis of the designed 2-(aryl/hetroaryl-hydrazono)-4,4-diphenylimidazolinones **3a–l, 4a–h,** and **5a,b** is outlined in *Scheme 1.* The key intermediate**,** 2-hydrazinyl-4,4-diphenyl-1*H*-imidazol-5(4*H*)-one **2,** was obtained by treatment of thiohydantoin **1** with hydrazine hydrate in refluxing EtOH [25]. The structure and physicochemical characteristics of **2** are consistent with the reported data [26]. The IR spectrum displayed the absorption bands characteristic for NH2, 2NH-, and -C=O groups at ~ 3440, 3324, 3228, 1724 cm^{-1}, respectively. The ^{1}H-NMR spectrum revealed two upfield singlets at δ = 2.10, and 3.57 ppm assigned to the terminal -NH$_2$, and -NH- protons of the hydrazine moiety respectively, and singlet at δ = 9.34 ppm of the imidazolinone -NH- proton.

The 10 protons of the diphenyl rings displayed multiplet at δ = 7.29 – 7.38 ppm.

The 2-(aryl/heteroarylmethylidene hydrazono)-4,4-diphenyl-1*H*-imidazolin-5(4*H*)-ones ,**3a – l,** were obtained by refluxing an ethanolic solution of 2-hydrazino-imidazolinone **2** with the appropriate aryl/heteroaryl aldehydes in presence of catalytic amount of glacial acetic acid analogous to reported method [27]. Likewise, treatment of **2** with the appropriate acetophenones or indoline-2,3-diones lead to the corresponding arylethylidenes **4a–h**, or 3-hydrazono-indolin-2-ones, **5a,b** respectively.

The structures of the synthesized hydrazones, **3a–l, 4a–h, and 5a,b,** were confirmed based on spectral and elemental analytical data. Their IR spectra revealed vibrations characteristic for imidazolinone - C=O (~ 1734–1710 cm^{-1}) and two -NH- bands at V = 3430–3220 cm^{-1}, in addition to bending and stretching vibrations of aromatic C-C and C-H bonds. The ^{1}H-NMR spectra (**Fig. SM8 – 29;** Supporting material) reveal disappearance of the NH$_2$ singlet at δ = 2.10 ppm characteristic for the starting agent, 2-hydrazinyl-diphenyl-1*H*-imidazolidinone **2**, and a concomitant downfield shift of the -NH- singlet from δ = 3.57 ppm to δ = 9.20 – 9.60 ppm, due to tautomeric nature. This behavior was previously reported in a series of 2-[(2-(phthalazin-1-yl)hydrazono)methyl]phenol and related derivatives [28]. However, the signals of the imidazolinone -NH- protons appear in a range of δ = 11.68 – 12.29 ppm indicating nonsignificant downfield shift relative to its position in the parent unsubstituted hydrazine **2**. Additionally, the spectra demonstrate distinctive signals for the respective compound classes. In case of the benzylidene series **3a–l**, the methine protons (-N=CH-) are clearly detectable at δ = 8.06 – 8.87 ppm. Alternatively, such singlets are missing in the spectra of the phenyl-ethylidine hydrazones **4a–h**, as well as the 3-hydrazono-indoline-2-ones **5a,b.** The protons of the diphenyl substituent linked to C-4 of the imidazolidinone nucleus and those of the phenyl moiety attached to the hydrazinyl linker appeared mostly as unresolved multiplets at δ ~ 6.90 - 8.33 ppm. In addition, characteristic signals of protons relating to specific function groups are detected e.g compound **3h** showed

two singlets at δ = 2.95 and 2.97 ppm due to N(CH$_3$)$_2$ moiety. However, compounds **3j** and **3k** displayed singlets of the methoxy substituents at δ = 3.82 and 3.78 ppm respectively.

Among series **4a-h**, compounds **4c** and **4g** displayed signals at δ = 2.35 and 3.78 ppm due to (CH$_3$) and (OCH$_3$) groups respectively. In addition, compounds **3i, 3j, 4d** and **4e** showed downfield shifted exchangeable protons due to (OH) and (NH$_2$) groups. The ^{13}C-NMR spectra (**Fig.s SM8–29;** Supporting material) illustrates some common characteristic signals due to imidazolinone C-atoms: C-2 (δ = 161.00), C-4 (δ = 71.49), C=O (δ = 176.0 ppm); and the azomethine C-atoms (-N=C̲H-) (δ = 144.99 - 148.89 ppm). The signals of remaining C-atoms appeared at the expected chemical shifts.
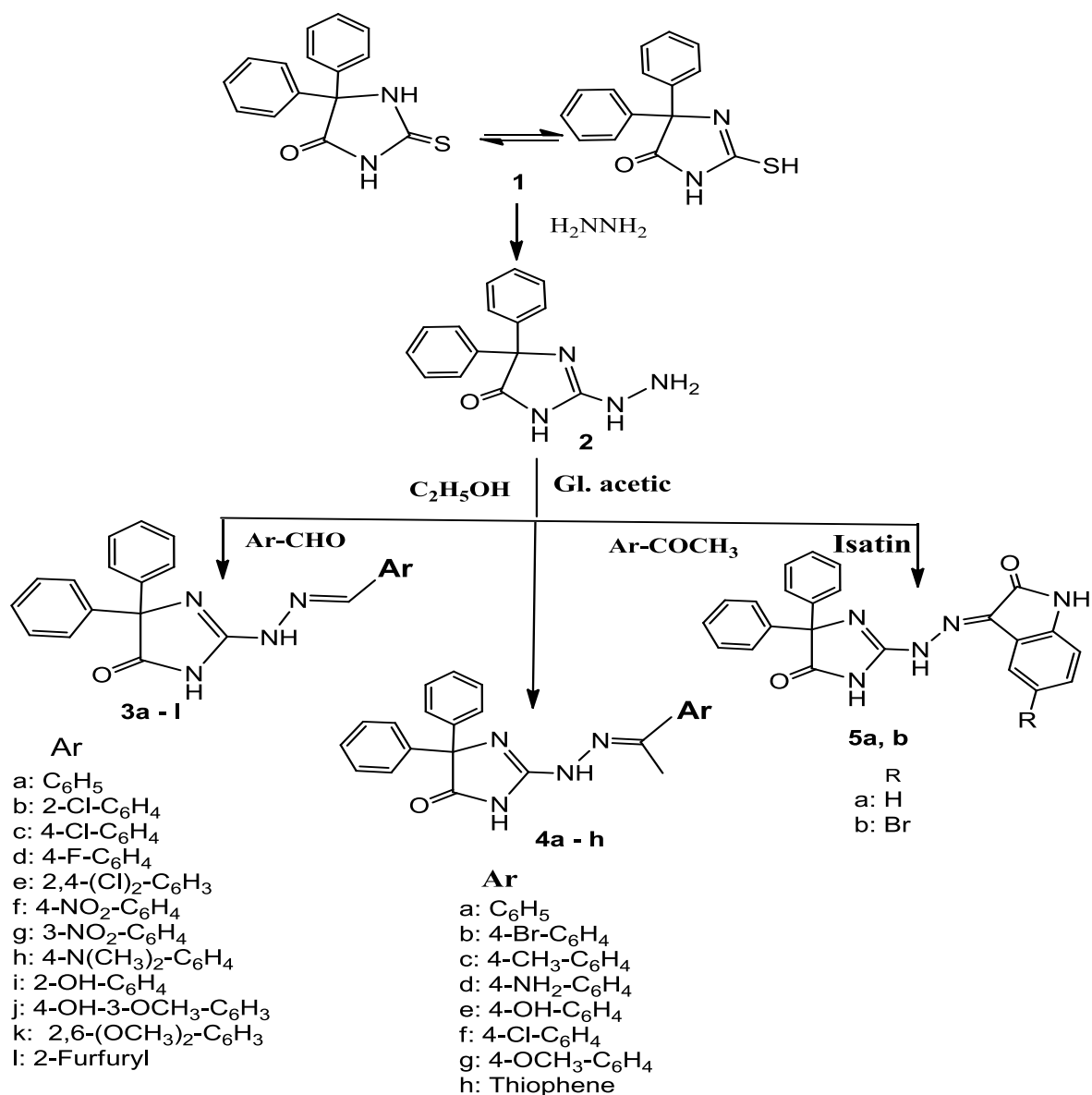
Biological evaluation
In-vitro antimycobacterial activity

The synthesized 2-(aryl/hetroarylhydrazono)-4,4-diphenylimidazo-linones **3a–l, 4a–h,** and **5a,b** were screened for their antimycobacterial activity against *M. smegmatis,* using broth microdilution method, in comparison to INH as reference drug. *M. smegmatis* (biosafety level 1) was utilized as a screening model. It is considered as the most appropriate for research analysis in laboratory experiments, being a "fast grower" and non-pathogenic mycobacterial stain[29]. It represents a good model to study mycobacteria in general and the highly pathogenic *M. tuberculosis,* since it shares the same peculiar cell wall structure as *M. tuberculosis* and other mycobacterial species[30,31]. Moreover, it shares more than 2000 homologous genes with *M. tuberculosis*[32].

The present investigation involves assessment of the primary effect on bacterial growth expressed as inhibition zone's diameter (IZD*: mm*). Furthermore, the minimal inhibitory concentration, (MIC*; µM*) and time-kill kinetics assay for compounds exhibiting meaningful inhibition zones (IZD > 10 mm) were also evaluated. The inhibition zones (**Fig. 3**) created by the tested compounds, at a concentration of 100 µg/well, illustrate that the benzylidene hydrazones **3a-l** have limited inhibition of *M. smegmatis.* Only compounds **3b**, and **3i**, showed comparable inhibition

zones, (IZDs = 17.5, and 14 respectively), to that of the parent hydrazine **2**. Remarkably, the arylethylidene hydrazones **4a-h** and the 2-oxoindol-3-yl hydrazones **5a,b** exhibit enhanced *in vitro* antimycobacterial activity. The inhibition zones of compounds **4a,b,c,e**, **5a** and **5b** were greater than that of the parent hydrazine **2** (IZDs ~ 17 – 24 *mm*). Obviously, the 2-oxoindolylhydrazone **5a** demonstrated the highest zone of inhibition of *M. smegmatis* (~ 24 mm), which is nearly equal to that of the reference drug INH. The minimum inhibitory concentrations (MIC*)* were determined for compounds displaying significant growth inhibition zones (*IZD* ≥ 10 mm), using broth microdilution method [33]. Two-fold decreasing concentrations (from 200 to 0.19 µg/ml) were tested. The results are summarized in **Table 1**, indicating that the arylethylidine hydrazones **4a**, **4c**, **4e**, and **5a** showed MIC values = 0.068, 0.033, 0.065, and 0.032 µ*M* respectively, that are comparable to that of the reference drug, INH (0.046 µ*M)*. Meanwhile, compounds **4f**, **4g**, **4h**, and **5b** showed MIC ranging from 0.106 – 0.134 µ*M*, accounting for 25 – 45% decreased potency than INH.

Scheme 1: Synthesis pathways of the designed compounds: 3a – l; 4a – h; 5a,b.

3a - l

Ar
a: C_6H_5
b: 2-Cl-C_6H_4
c: 4-Cl-C_6H_4
d: 4-F-C_6H_4
e: 2,4-$(Cl)_2$-C_6H_3
f: 4-NO_2-C_6H_4
g: 3-NO_2-C_6H_4
h: 4-$N(CH_3)_2$-C_6H_4
i: 2-OH-C_6H_4
j: 4-OH-3-OCH_3-C_6H_3
k: 2,6-$(OCH_3)_2$-C_6H_3
l: 2-Furfuryl

4a - h

Ar
a: C_6H_5
b: 4-Br-C_6H_4
c: 4-CH_3-C_6H_4
d: 4-NH_2-C_6H_4
e: 4-OH-C_6H_4
f: 4-Cl-C_6H_4
g: 4-OCH_3-C_6H_4
h: Thiophene

5a, b

R
a: H
b: Br

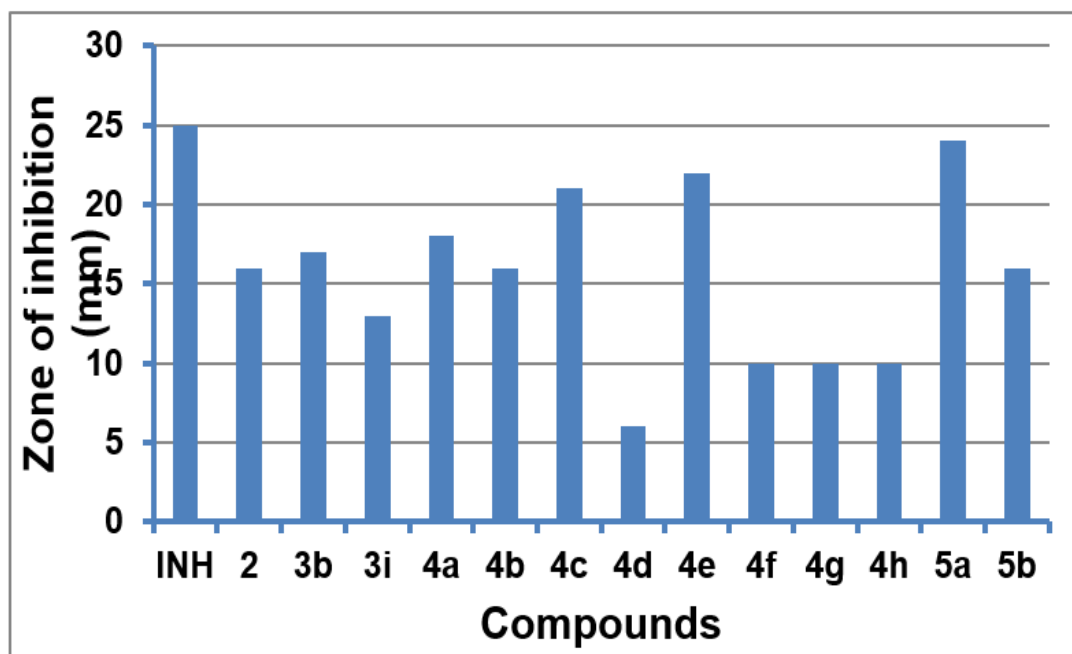**Scheme 1:** Synthesis pathways of the designed compounds: 3a – l; 4a – h; 5a,b.

Fig. 3: Inhibition zones of the tested compounds.

Table 1: Antimycobacterial activity and cytotoxicity (CC_{50}) of the studied compounds and INH.

Code	Aryl/heteroaryl	IZD (mm)	MIC (µM)*	CC_{50}^{a} (µM) (SI[b])
2	H	16	0.188	
3b	2-Cl-Phenyl	17	> 0.515	
3i	2-OH-Phenyl	13	> 0.540	
4a	Phenyl	18	0.068	26.93 ±5.4 (396.0)
4b	4-Br-Phenyl	16	0.447	
4c	4-CH₃-Phenyl	21	0.033	71.11 ±5.9 (2155)
4d	4-NH₂-Phenyl	6	> 50	
4e	4-OH-Phenyl	22	0.065	8.91 ±0.4 (137.1)
4f	4-Cl-Phenyl	10	0.124	
4g	4-OCH₃-Phenyl	10	0.130	
4h	2-Thienyl	10	0.134	
5a	2-Oxoindol-3-yl	24	0.032	27.84 ±2.3 (870)
5b	5-Br-2-Oxoindol-3-yl	16	0.106	11.46 ±2.4 (108.1)
INH	----	25	0.058	

*: All measurements were done in triplicate.

[a]: The concentration of the tested compound reduces the cell viability by 50%.

[b]: Selectivity index is the ratio of CC_{50}/MIC.

Time-kill kinetics

Assessment of time-kill kinetics is routinely applied to allocate the observed antimicrobial activity of tested molecules as bacteriostatic or bactericidal against specific bacterial strain. This is achieved predominantly by counting the viable bacterial cells at serial two-fold dilutions of the tested compounds after specific time intervals in a 96-well microtiter plate [34]. Generally, a reduction in CFU/ml of < 3log value of the initial count, during incubation period of 24 h, indicates bacteriostatic activity, whereas a value of ≥ 3log decrease designates bactericidal activity [35]. In this study, the time-kill kinetics of selected compounds including the unsubstituted imidazolyl-2-hydrazine **2**, 2-Hydroxybenzylidene hydrazone **3i**, 4-tolyl-ethylidene hydrazone **4c**, and 2-oxoindoline-*3*-hydrazone **5a** were evaluated in comparison to the reference drug INH. The results are depicted in **Fig. 4**, demonstrating clearly that compound **5a** showed a killing-kinetics pattern almost identical to that of INH. The other compounds **2**, **3i** and **4c** suppress the proliferation of *M. smegmatis* and maintained the initial bacterial count almost unchanged (**Fig. 4A**). Unequivocally, compound **5a** as well as INH displayed > 1 log reduction (~ 90 % killing) of the initial population of the cells and marginally < 2 log reduction (~ 99% killing) at 2xMIC after 48 h. and 72 h. of treatment, respectively, indicating bacteriostatic effect. Alternatively, at 4xMIC both compounds **5a** and INH exhibited ≥ 3 log reduction, (**Fig. 4B**), of bacterial count (~ 99.9 % killing) after 72 h, illustrating bactericidal effect. Compounds **2** and **4c** showed only 1 log reduction after 72 h of treatment, while bacterial count remained constant in culture treated with compound **3i** at all time intervals.

In-vitro cytotoxicity study

Cytotoxicity assessment represents a prime requirements for investigational compounds showing antimicrobial efficacy. This study is done to highlight the of the tested compounds on the host normal cells. Consequently, the compounds exhibiting significant antimycobacterial activity (**4a,c,e and 5a,b**) with MIC values ≤ 0.20 *μM* were tested for potential toxic effects on normal kidney epithelial cells derived from African green monkey (Vero cells) using MTT (3-(4,5-Dimethylthiazol-2-yl)-2,5-diphenyl tetrazolium bromide) assay. The method depends on colorimetric assessment of the decrease in color intensity of insoluble purple formazan crystals resulting from reduction of the tetrazolium salt. This effect is due to inhibition of certain enzymes responsible for cellular viability [36]. The produced formazan crystals are then dissolved using a solubilizing solution e.g. isopropyl alcohol and the absorbance is measured at 500 - 600 nm using plate-reader. The darker the solution, the greater the number of viable cells.
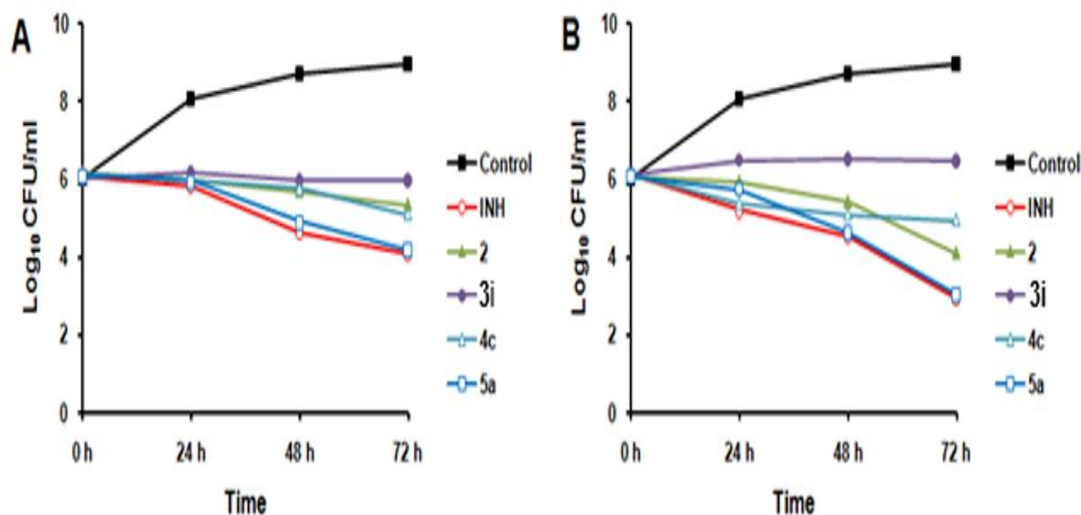

Fig. 4: Time-kills assay results against *M. smegmatis*. A: 2xMIC; B: 4xMIC

The cytotoxicity results (CC$_{50}$ in μM) and the respective selectivity index (*SI*) of the tested compounds are presented in **table 1**. *SI* is the ratio of *in vitro* cytotoxicity (CC$_{50}$ μM) to antimycobacterial activity (MIC in μM). It now generally accepted that, candidate compounds are considered as nontoxic antimycobacterial, if the *SI* value is $\geq$ 10, with MIC value lower than 6.25 mg/ml [37]. The results indicate that the calculated *SI* values (**Tab. 1**) of the tested compounds ranging from 108.1 to 2155, demonstrating higher safety margin to the host cells.

Structure activity relationship (SAR) study

This study is executed to explore the impact of the structural fragments of the designed compounds on the observed antimycobacterial activity. The results (**Fig. 5**) demonstrate that derivatization of diphenylimidazolinone-2-hydrazine **2** to the corresponding arylidene hydrazones results generally in enhancement of the antimycobacterial activity. Comparison of the studied series **3a–l**, **4a-h**, and **5a, b** indicates that the arylethylidenes **4a-h** and the indolinones **5a, b** surpassed their benzylidene analogues **3a-l**. A plausible explanation for this difference could be attributed to the presence of CH$_3$ substituent at the α-C atom of the hydrazone moiety in case of aryl ethylidenes **4a-h**, which confers bulkiness attaining proper

orientation of the binding groups in the active site of the target enzyme. The bending substituents on the arylidene moiety demonstrate variable effects on the observed antimycobacterial activity. The MIC values of the arylethylidenes **4a-h** indicate that compounds having electron donating substituents: **4c** (4-CH$_3$), and **4e** (4-OH) are more potent, (MIC values: 0.033, and 0.065 μM, respectively), than the corresponding analogs with electron withdrawing substituents e.g. **4b** (4-Br), and **4f** (4-Cl): MIC values: 0.447, and 0.124 μM, respectively.

Bioactivity profiling and molecular modeling

Several computational approaches have been developed for prediction of putative targets of many newly developed molecules as well as isolated natural products. This is considered as an interesting tactic specially in demanding resources to perform enzymatic assays. In the present investigation, some of these computational and in silico applications were explored to delineate the potential molecular target(s) involved in the observed antimycobacterial activity of the studied compounds (**3a–l**, **4a-h**, and **5a,b**). A stepwise analysis compressing both 'reverse or inverse' ligand-based and structure-based approaches have been accomplished [38,39].
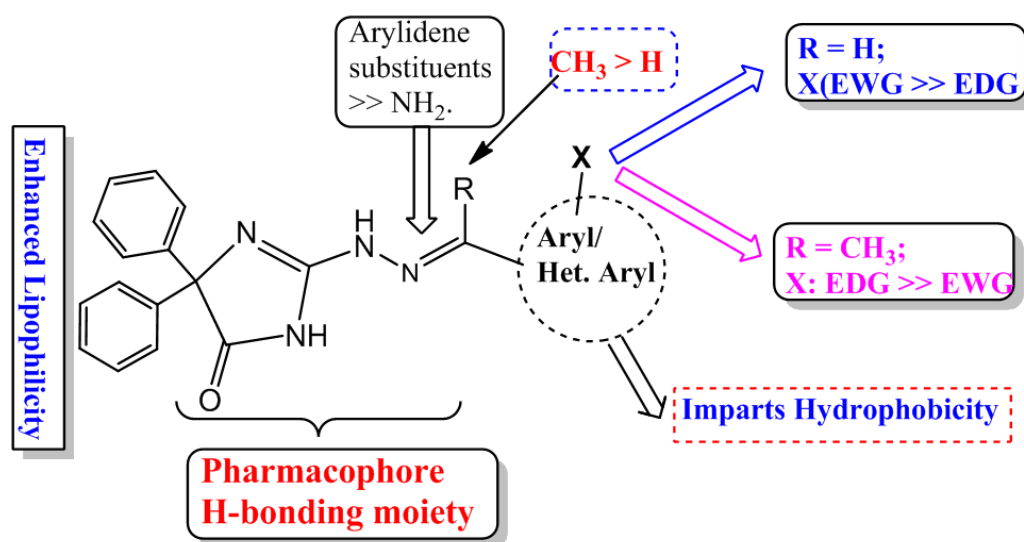

Fig. 5: Summary of the SAR of the studied antimycobacterial compounds.

Shape-based similarity analysis

ChemMine tools is an online service involving a web interface to a set of cheminformatics and data mining tools that are useful for various analysis routines performed in chemical genomics and drug discovery. Several approaches were developed e.g., similarity searching, which includes pairwise matching of structural fragments among compounds, and the result is expressed as numerical similarity index [40]. Informatics resources in these areas are essential for exploring the structure, properties, and bioactivity of biologically relevant molecules. Additionally, this might assist the process of target fishing relevant to respective mechanism of action [41]. In the present investigation, we applied shape-based similarity (Tanimoto coefficient) approach for assessment of the similarity index between the most active compounds (**4c** and **5a**) and a set of selected hydrazone and/or amide-based related compounds, **A – H** (**Tab. 2**). The selection criteria based principally on experimentally reported antimycobacterial activity combined with successful docking into a recognized mycobacterial target. Explicitly, inhibitors of acyl carrier protein reductase (InhA), Mycobacterial membrane proteins Large (MmpL3**),** Pantothenate Synthetase (PS), β-ketoacyl acyl-carrier-protein synthase III (FabH), and Cytochrome P450 (CYP121A1). The results revealed that compounds **B - H** showed similarity indexes in the range of 0.189 – 0.458. However, compound **A** targeting acyl-carrier-protein reductase (InhA), showed the lowest Tanimoto coefficient, hence, it is excluded from the next step.

Table 2: Atom pair (AP) Tanimoto similarity indexes with compounds 4c and 5a using ChemMine tools.
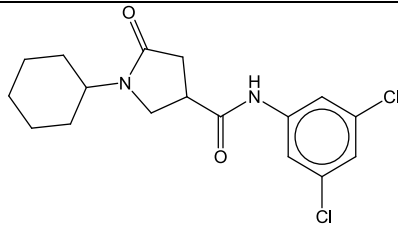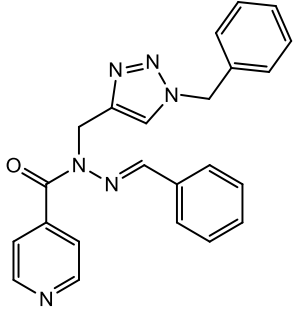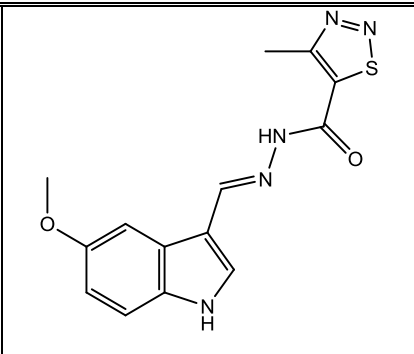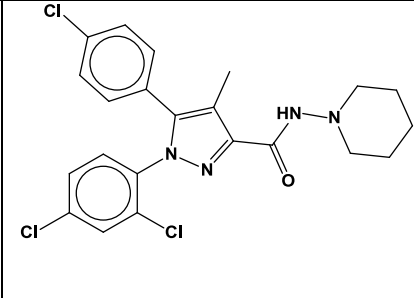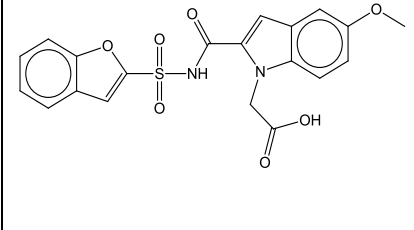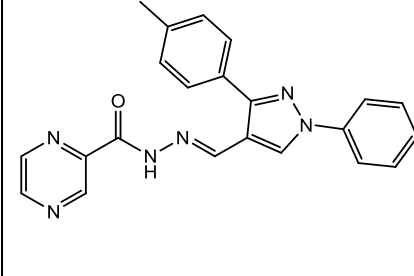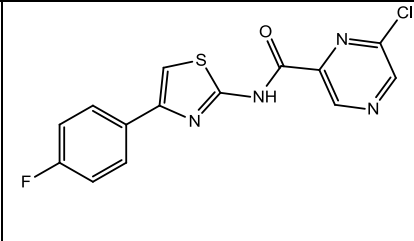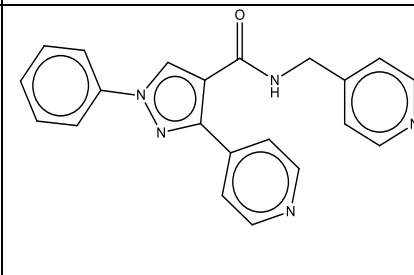
Code	Structure	AP (4c)	AP (5a)	Mycob. target	Lit.
A)		0.068	0.073	InhA	**42**
B)		0.290	0.302	InhA	**43**

Table 2: Continued.

C)		0.235	0.209	InhA	**44**
D)		0.198	0.189	MmpL3	**45**
E)		0.242	0.241	PS	**46**
F)		0.458	0.425	PS	**47**
G)		0.247	0.247	FabH	**48**
H)		0.340	0.326	CYP121A1	**49**

Pharmacophore mapping

Pharmacophore mapping is a broadly used ligand-based method in drug target identification. In this respect, the adopted target fishing phases involves application of "reverse pharmacophore mapping" approach, for elucidation of the potential mycobacterial target of the studied compounds [39]. Firstly, a pharmacophore model, derived from the investigated compounds (**4a, c, e-g and 5a, b**) as training set was generated using the pharmacophore elucidator module of the software Molecular Operating Environment, (MOE 2020.01, https://www.chem-comp.com). This is followed by testing against a database set compressing the structures **B – H (test set)**, which displayed significant Tanimoto similarity indexes (**Tab. 2**). The procedure involves initial flexible alignment of the training set molecules, to assign scores to the respective generated queries. The score is based on a shared measure of their cover, how many compounds were used to generate the model out of the initial set, overlap, how well they applied the ligands, and accuracy, how well they group the dataset into actives and inactives [47]. The respective values for the generated pharmacophore queries of the training set compounds reveal the cover = 7 compounds out of 7, overlap = 6.11, accuracy = 1.0, (**Table SM1,** supporting material). The following pharmacophoric features (**Fig. 6A**) were allocated within the training set compounds: two potential aromatic ring centers (F1 and F2, green spherical meshes), and H-bond acceptor (F3, cyan spherical mesh). **Fig. 6B** illustrates the overlay of the training set molecules to the generated pharmacophore model. The validity of the model has been also assessed against a database set including the least active tested compounds (**3b, 3i, and 4b),** with MIC values higher than 0.4 µM (**Tab. 1**). The results identified 3 hits, (**Table SM2**), with rmsd values = 0.05, 0.02, and 0.02 respectively, reflecting the reliability of the generated pharmacophore model (**Fig. SM1**).

Mapping the test set compounds **B – H**, (**Table 2**), to the generated pharmacophore model revealed that six of them (**B, C, E, F, G and H**) are aligned with acceptable root-mean-square distance (rmsd) values, (**Table SM3**). Analysis of the obtained results indicates that compounds **B** and **C** displayed rmsd value = 0.950 and 0.445, respectively. Both compounds are inhibitors of mycobacterial InhA, however compound **B** has higher RMSD value than **C**, hence, it was disregarded. Likewise, compounds **E** and **F** are reported pantothenate synthetase inhibitors. Compound **E** showed a lower RMSD value (0.490) than **F** (RMSD = 0.681). Moreover, (**E**) is the native ligand of pantothenate synthetase [46], hence selected for the next step. Consequently, the results of reverse pharmacophore mapping analysis indicate that compounds **C, E, G,** and **H, (Tab. 2**), aligned adequately with the generated pharmacophoric model (**Table. 3**). The assigned targets for these compounds are acyl-carrier protein reductase InhA, Pantothenate synthetase, ß-ketoacyl acyl-carrier-protein synthase III FabH, and CYP121A1, respectively.

Furthermore, we utilize the flexible alignment plate form to explore the possible matching of the 3D structures of the training set compounds (**4a, c, e-g and 5a, b**). The results show high grade placement with least strain energy (U = 64.44, F = -224.51, S = -160.07) (**Fig. SM2**). Interestingly, appropriate alignments were also documented between the investigated compounds (training set) and the top-scored test set compounds **C, E, G,** and **H (Tab. 3),** as depicted in **Fig. SM3,** supplementary material**.** The results of reverse pharmacophore mapping and flexible alignment illustrate that the designed compounds (**4a, c, e-g and 5a, b**) might bind to the proposed targets of the selected hits, (**C, E, G and H**), in a comparable set of interactions. Accordingly, the obtained results provide virtual evidence for the multitarget potential of the studied compounds.
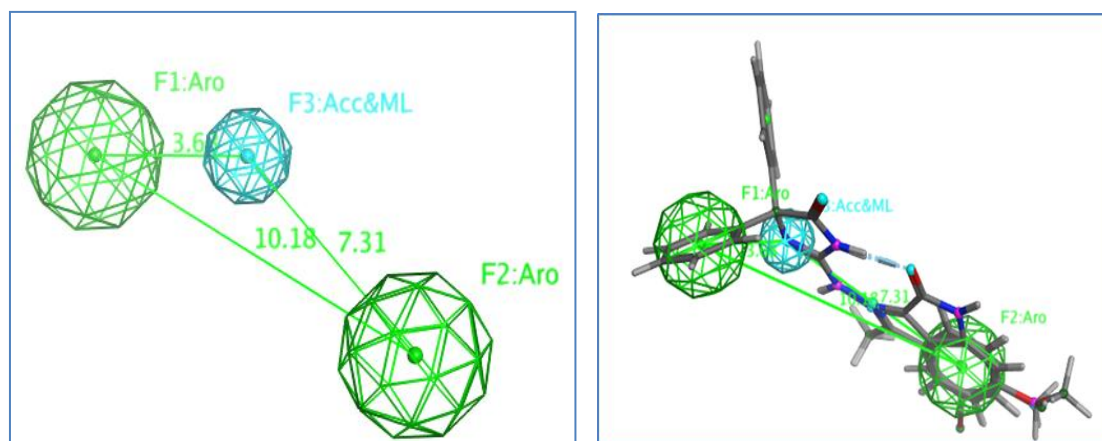
Fig. 6 A: The derived Pharmacophore model.   **B:** Overlay of the training set compounds (4a, c, e-g and 5a, b) on the pharmacophore Model.

Table 3: Pharmacophore mapping and Flexible alignment results of the hit structures.

Code	RMSD (Å)	Mycob. target	Flexible alignment Score	
			4c	5a
C	0.449	InhA	- 60.37	-36.86
E	0.490	PS	-146.38	-121.14
G	0.543	FabH	-81.48	-60.72
H	0.801	CYP121A1	-84.42	-61.44

Inverse docking study

Inverse docking represents the most popular tool mainly in drugs repurposing studies. It offers a useful approach to drug discovery. Obviously, reverse docking is a known target fishing tool involving exploration of binding complementarity between sets of small molecule ligands and a panel of selected clinically validated biological targets. The result offers a list of targets ordered according to scoring functions. Targets demonstrating the highest scores represent reliable candidates for potential interaction with the ligands [50]. Application of this approach designates the last step in the present study aiming to rationalize mechanism-based evidence for the observed antimycobacterial activity elicited by the studied compounds **3a-l, 4a-h,** and **5a, b**.

Based on the results of Shape-based similarity analysis (**Tab. 2**), pharmacophore mapping, and flexible alignment (**Tab. 3**), we could assign four different potential mycobacterial targets. Namely, acyl-carrier protein reductase (InhA), pantothenate synthetase (PS), β-ketoacyl acyl-carrier-protein synthase III (FabH), and cytochrome CYP121A1. Accordingly, an inverse docking study was achieved involving compounds **4a,c,e** and **5a,** that showed MIC values ranging from 0.03 – 0.06 *uM* against *M. smegmatis.* The X-ray crystal structures of the assigned mycobacterial targets were obtained from, protein data bank (PDB), are listed in **table 4**. Primarily, method validation was performed by redocking the respective native ligands reported for each target and assessing the root mean square deviation (rmsd). The analytical potential of a computational module is verified by rmsd value < 1.5 Å. Superimposition of the respective native ligands and their redocked pose are shown in **Fig.**s **SM4(A-D),** supporting material.

Table 4: Inverse docking scores (S, Kcal/mol), and the ranking of the most active compounds (4a, c, e and 5a) against the selected mycobacterial targets.

Ligands	Docking Scores (ranking)				MIC (uM)
	4TZK	**3IVX**	**IU6S**	**6GEQ**	
4a	-13.07 (4)	-11.95 (4)	-12.44 (4)	-12.05 (4)	0.056
4c	-14.95 (2)	-12.36 (3)	-13.00 (3)	-14.55 (2)	0.031
4e	-15.71 (1)	-13.67 (1)	-14.45 (1)	-14.95 (1)	0.062
5a	-14.42 (3)	-12.94 (2)	-13.78 (2)	-13.00 (3)	0.026
Mean S.[a]	**-14. 54 (1st)**	**-12.73 (4th)**	**-13.41(3rd)**	**-13.63 (2nd)**	
Nat. Lig.[b]	**-11.75**	**-18.89**	**-21.33**	**-12.74**	

4TZK: acyl-carrier protein reductase InhA; **3IVX:** pantothenate synthetase; **IU6S:** β-ketoacyl acyl-carrier-protein synthase III (FabH); **6GEQ:** (CYP121A1).
[a]: Mean of docking Score values.
[b:] Docking scores of the co-crystallized ligand (Native ligand).

The docking results were interpreted based on docking scores, total number and type of hydrogen bonds and hydrophobic interactions with the respective target. Analysis of the docking results revealed that the studied compounds, **4a,c,e** and **5a**, indicate analogous interactions with the selected targets. Comparing the docking ranks (**Table 4**) to the *in vitro* antimycobacterial activity revealed that the unsubstituted benzylethylidene hydrazone **4a,** showed the lowest binding affinity, (4th rank), to the studied mycobacterial targets. Alternatively, the 4-hydroxy congener **4e** displayed the top docking scores (1st rank) within the four targets. Meanwhile, the docking scores of the p-tolylethylidene derivative, **4c** and the 2-oxoindolyl derived hydrazone, **5a** showed almost equal docking scores. Additional ranking parameters based on calculating the mean values of docking scores elicited by the four compounds for each target (**Table 4**) also provide additional validating evidence. The results indicate that mycobacterial acyl-carrier-protein reductase InhA (PDB: **4TZK**) is the most credible target, followed by cytochrome CYP121A1 (PDB: **6GEQ)**, β-ketoacyl acyl-carrier-protein synthase III FabH (PDB: **IU6S**), and pantothenate synthetase (PDB: **3IVX**), respectively.

Docking into the active site of acyl-carrier-protein reductase (InhA)

Based on the previously discussed results of the assumed sequential analysis it could be concluded that acyl-carrier-protein reductase (InhA) is the most credible target for the observed antimycobacterial effect of the studied compounds. Subsequently, it was interesting to accomplish a exhaustive docking study of the most active compounds, **4a,c,e** and **5a,** into the active site of this enzyme to explore the binding modes and the critical amino acid residues involved in interactions with the designed inhibitors.

ACP reductase belongs to the tyrosine dependent oxidoreductase family and depends on *NADH* as a cofactor [4]. Its crystal structure in complex with *NAD⁺* and a fatty acyl substrate shows that the later binds in U-shaped conformation and consists of the amino acid residues: Phe149, Tyr158 and Lys165, (**Fig. SM5**, supporting material), that are assigned as catalytic triad and found to be fundamental for trans-enoyl reduction catalysis [51]. Additionally, a set of hydrophobic residues are in the substrate binding loop (*SBL)* involving Met103, Phe149, Thr196, Met199, Leu207 and Ile215[52,53].

The crystallographic structure of enoyl ACP reductase (InhA), co-crystallized with 1-cyclo-hexyl-4-dichlorophenylpyrrolidine-2-one carboxamide **III** (PDB code: 4TZK), is downloaded from PDB, http://www.rcsb.org. The proposed docking algorithm was validated by redocking of the native ligand into the target protein (*InhA)*. The respective validation criteria in this study showed rmsd value = 0.8343 Å and the docking score = -11.34 kcal/mole, (**Fig. SM4A**, supporting material). The results (**Table 5**) display docking scores for compounds, **4a,c,e** and **5a**, ranging from -13.07 to -15.71 *Kcal/mol,* suggesting higher affinity than the co-crystallized ligand (11.34 *Kcal/mol)*. The respective interactions with the amino acid residues in active site are almost

analogous to those elicited by the native ligand. Essentially, H-bonding, π-H, π-cation, as well as hydrophobic interactions with Tyr158, Lys165, Phe149, Met103, which are crucial for enzyme inhibition. **Fig.**s **7** and **8** demonstrate the 2D and 3D docking representations of compounds **4c** and **5a**, respectively. Furthermore, the respective **Fig.**s illustrating the 2D and 3D interactions of compounds **4a** and **4e** are presented in **Fig.s SM6** and **SM7** in supporting material.

Molecular characteristics and drug-likeness

Molecular features denote a balance of the respective structural moieties that verify the coherence of drug molecules. Lipophilicity, molecular volume, flexibility, and presence of various pharmacophoric groups are the main physicochemical properties that influence the behavior of molecules in a living organism. Good bioavailability can be achieved with an appropriate balance between solubility and partitioning properties. Thus, the compliance of the synthesized compounds to Lipinski's rule of five was computationally investigated [54]. In addition, topological polar surface area (TPSA)

and the number of rotatable bonds (# rotb) are correlated to drug bioavailability [55-57].

Consequently, the mentioned characteristics of the studied compounds were calculated using the online free *Molsoft* and *Molinspiration* software and compared to the values of the reference drug, INH (**Table 6**). The results indicate that all the investigated compounds displaying TPSA values < 140Å^2, and 3 – 6 rotatable bonds suggesting higher possibility of intestinal absorption. This has been augmented by enhanced lipophilic characteristics of the studied compounds (Log P = 3.61 - 4.91).

The drug likeness score combines Log P, solubility, molecular weight, and toxicity risks in one handy value that may be used to afford the overall potential to qualify for a drug [56]. A value of 0.5 or more implies that a compound is a promising lead for future development and optimization. The overall drug score values for the studied compounds were calculated using molsoft software (*http://molsoft.com/mprop*) and compared to that of the reference drug, INH. The data (**Table 6**) revealed that the studied compounds showed acceptable drug-like score values.

Table 5: Docking results of the most active compounds and the native ligand III into Enoyl-acyl carrier protein reductase (InhA), (PDB: 4TZK)

Comp.	Score (S)	# of H-bonding interact.	# Arene-H interactions
Native ligand*	-11.34	3 HBD (Met103,161), 2 HBA (Tyr158, Leu218)	2 (Tyr 158, Ile215)
4a	-13.07	HBA (Gly96)	Ile95, Met161
4c	-14.95	2 HBD (Met155), HBA (Tyr158)	Tyr158, π-cation (Lys165)
4e	-15.71	HBA (Lys165)	3 (Ile95, Tyr158, Phe149)
5a	-14.42	2 HBA (Lys 165, Ile194)	Phe149

* 1-cyclo-hexyl-4-dichlorophenylpyrrolidine-2-one carboxamide **III.**

Fig. 7: Binding pattern of **4c** (in violet) and its overlay with the native ligands (in green) into ACP reductase active site (PDB 4TZK); 3D (left panel) and 2D (right panel).

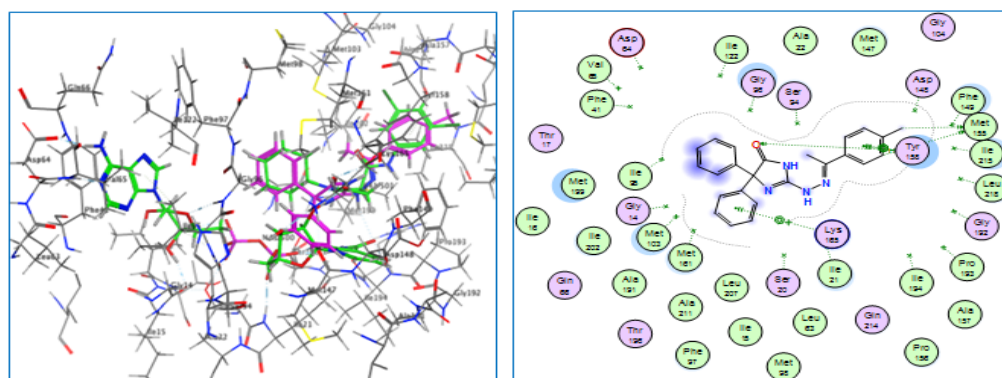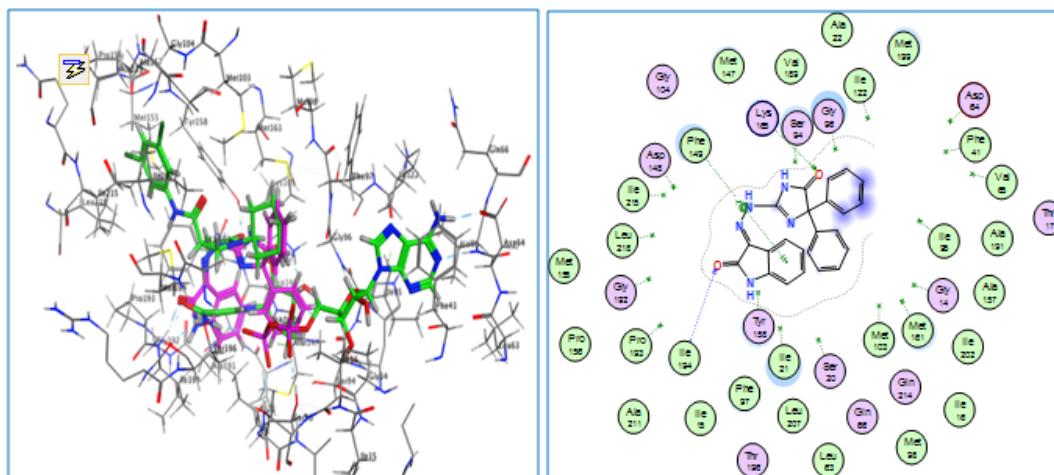**Fig.** 8: Binding pattern of 5a (in violet) and its overlay with the native ligands (in green) into ACP reductase active site (PDB 4TZK); 3D (left panel) and 2D (right panel).

Table 6: Computational molecular characteristics of the most active compounds in comparison to the reference drug (INH).

Comp. #	M. Wt.	cLogP	TPSA	#rtb	Lip. acc.	Lip. don	# viol.	Drug-Like score
4a	368.44	4.41	57.17	5	5	3	0	1.00
4c	382.47	4.55	65.85	5	5	2	0	1.00
4e	384.44	3.63	74.79	5	6	2	0	1.00
4f	402.89	4.78	65.85	5	5	3	0	1.00
4g	398.47	4.16	75.09	6	6	2	0	1.00
4h	374.47	4.89	65.85	5	5	2	0	1.00
5a	396.45	3.61	81.69	4	6	2	0	1.00
5b	475.34	4.52	81.69	4	6	3	0	1.00
INH	137.14	-0.97	68.01	2	4	3	0	1.00

cLog P*: lipophilicity parameter, **TPSA***: topological polar surface area, **rt**: rotatable bonds.

Conclusion

Three sets of 4,4-diphenylimidazolinone-derived hydrazones **3a-l, 4a-h, and 5a,b** were designed, synthesized, and tested as potential antimycobacterial activity against *M. smegmatis*. The benzylidene hydrazones **3a-l** exhibited limited antimycobacterial activity, whereby only compounds **3b** and **3i** showed moderate activity (MIC values: ~ 0.13 - 0.54 *μM* respectively). Alternatively, the phenylethylidenes **4a-h** and indolinone hydrazones **5a,b** demonstrated enhanced activity (MIC values: 0.032 – 0.45 *μM).* Remarkably, the results of the time-kill assay revealed that compound **5a** demonstrated bactericidal activity against *M. smegmatis* comparable to that of INH. Computational biological profiling approaches were adopted for assessment of plausible target(s) for the most active compounds. The results demonstrate multitarget potential of the investigated compounds. Sequential analysis of the predicted targets revealed that enoyl ACP reductase (InhA) is the most credible target accounting for the observed activity. This result is assisted by molecular docking study on the active site of the putative target, illustrating that the tested compounds bind to the active site of InhA (PDB: 4TZK) in an analogous manner to that of the native ligand. Moreover, computational assessment of the molecular properties and drug-like score revealed that the studied compounds are complying with the conventional characteristics of investigational

drugs. The results suggest that the studied arylidene hydrazinylimidazolinones are contenders for further testing and/or optimization as antimycobacterial therapeutics.

Experimental
Chemistry

The IR spectra were recorded in potassium bromide discs on a PyeUnicam SP 3300 Shimadzu FT IR 8101 PC infrared spectrophotometers. ^{1}H-NMR (400 MHz) and ^{13}C-NMR (100 MHz) were run in deuterated dimethylsulphoxide (DMSO-$d6$). Elemental analyses carried out at the Regional Center for Mycology and Biotechnology, Al-Azhar University, Cairo/Egypt. All reactions were monitored by TLC (Silica gel, Aluminum Sheets 60 F254, Merck), using petroleum ether/ethyl acetate at appropriate proportion to separate the products. The following intermediates and/or final compounds were prepared according to the assigned reported methods:**1**[25]; **2,3a,b,c,e,f,i,j**[26]; **4a** [27].

Synthesis of Arylmethylidenehydrazones (3a–l)

A mixture of 2-Hydrazinyl-4,4-diphenyl-1H-imidazol-5(4H)-one **2** (2.5 mmol) and the appropriate arylaldehyde (2.5 mmol) in ethanol (20 mL) and few drops of glacial acetic acid (~1 mL) was heated under reflux for 6 – 20 h, as monitored by TLC. The reaction mixture was then cooled and diluted with water. The formed solid product was then collected by filtration, dried, and recrystallized from ethanol (unless otherwise specified) to afford the corresponding arylhydrazones **3a–l.** % Yield, reaction time, melting points, spectral & elemental data are listed below.

Diphenyl-2-[(phenylmethylene)hydrazono]-1H-imidazol-5(4H)-one (3a)

White powder (60 %), 9 h, MP. 297°C (Lit. 240–242°C) [26]. IR v cm^{-1}: 3341, 3150 (2NH), 1735 (CO). ^{1}H-NMR, δ ppm: 7.33 – 7.43 (m,13H, diphenyl and benzylidene-H3,4,5), 7.88 – 7.90 (m, 2H, benzylidene-H2,6), 8.20 (s, 1H, N=CH), 9.55 (s, 1H, -NH-N=, D$_2$O exchange), 11.76 (s,1H, im-NH, D$_2$O exchange). ^{13}C-NMR, δ ppm: 71.48 (im-C-4), 126.66, 127.12, 127.41, 127.48, 127.66, 127.91, 128.23, 128.44, 128.52, 129.81, 134.62, 140.54, 145.49 (aromatic C-atoms),

148.89 (N=$\underline{CH}$). Anal. Calcd. for C$_{22}$H$_{18}$N$_4$O (354.41) C, 74.56; H, 5.12; N,15.81. Found: C, 74.69; H, 4.88; N, 16.04 %.

[(2-Chlorophenylmethylene)hydrazono]-4,4-diphenyl-1H-imidazol-5(4H)-one (3b):

White powder (80 %),12 h, MP. 299-300°C, (204–206°C) [26]. IR v cm^{-1}: 3444, 3163 (2NH), 1755(CO).^{1}H NMR, δ ppm: 7.34 –7.49 (m, 13H, diphenyl and benzylidene H3,4,5), 8.39 – 8.49 (m, 1H, benzylidene H-6), 8.56 (s, 1H, N=CH), 9.63 (s, 1H, -HN-N=, D$_2$O exchange), 11.79 (bs, 1H, im-NH, D$_2$O exchange). ^{13}C NMR, δ ppm: 71.40(im-C-4), 126.66, 127.11, 127.19, 127.81, 127.89, 128.00, 128.29, 128.49, 129.50, 129.71,130.5, 131.20, 131.78, 132.56, 132.87, 140.33, and 144.99 (aromatic C), 145.49 (N=$\underline{CH}$). Anal. Calcd. For C$_{22}$H$_{17}$ClN$_4$O (388.86) C, 67.95; H, 4.41; N, 14.41. Found: C, 68.63; H, 4.33; N, 14.56 %.

[(4-Chlorophenylmethylene)hydrazono]-4,4-diphenyl-1H-imidazol-5(4H)-one (3c)

White powder (95 %),6 h, MP. 290°C (decomp.), (lit. 280–282, Dioxane)[26]. IR vcm^{-1}: 3250, 3163 (2NH), 1747 (CO). ^{1}H-NMR, δ ppm: 7.32 – 7.49 (m, 12H, diphenyl and benzylidene H3,5), 7.91 – 7.93 (d, J ~ 8Hz, 2H, benzylidene H2,6), 8.20 (s, 1H, N=CH), 9.54 (s, 1H, -HN-N=, D$_2$O exchange), 11.65 (bs, 1H, im-NH, D$_2$O exchange). ^{13}C-NMR, δ ppm: 71.36 (im-C-4), 126.66, 127.77, 127.95, 128.27, 128.39, 128.47, 128.58, 129.01, 129.11, 133.76, 134.17, 140.44, 147.97 (aromatic C-atoms), 148.89 (N=$\underline{CH}$). Anal. Calcd. for C$_{22}$H$_{17}$ClN$_4$O (388.86) C,67.95; H, 4.41; N, 14.41. Found: C, 67.74; H, 4.31; N, 14.60 %.

[(4-Fluorophenylmethylene)hydrazono]-4,4-diphenyl-1H-imidazol-5(4H)-one (3d)

White powder (80 %),12 h, MP. >300°C (decomp.). IR v cm^{-1}: 3405, 3215 (2NH), 1742 (CO). ^{1}H-NMR, δ ppm: 7.19 – 7.42 (m, 12H, diphenyl and benzylidene H3,5), 7.93 – 7.98 (m, 2H, benzylidene H2,6), 8.20 (s, 1H, N=CH), 9.52 (s,1H, -HN-N=, D$_2$O exchange) 11.70 (bs, 1H, im-NH, D$_2$O exchange). ^{13}C-NMR, δ ppm: 71.39(im-C-4), 115.44, 115.65, 126.66, 127.10, 127.63, 127.93, 128.26, 128.45, 129.40, 129.60, 129.68, 131.34, 140.51, 140.63 (aromatic C-atoms), 147.87 (-

N=$\underline{CH}$), 161.80 (im C=N), 164.62 (C=O). Anal. Calcd. for $C_{22}H_{17}FN_4O$ (372.39): C, 70.96; H, 4.60; N, 15.04; Found: *C,* 70.97; H, 4.52; N, 15.15%.

Diphenyl-2-[(2,4-dichlorophenylmethylene) hydrazono]-1*H*-imidazol-5(4*H*)-one (3e)

White powder (85 %),12 h, MP. > 300°C decomp., (Lit. 244–246 °C) [26]. IR ν cm^{-1}: 3225, 3210 (2NH), 1745 (CO). ^{1}H-NMR, δ ppm: 7.29 - 7.50 (m, 11H, diphenyl and benzylidene H-5), 7.62 – 7.68 (m, 1H, benzylidene H-3), 8.42 (d, J ~ 8 Hz, 1H, benzylidene–H-6), 8.48 (s, 1H, N=CH), 9.64 (s,1H, -HN-N=, D_2O exchange), 11.92 (bs, 1H, im-NH, D_2O exchange). ^{13}C NMR, δ ppm: 71.34(im-C-4), 126.66, 127.09, 127.52, 127.87, 128.03, 128.33, 128.51, 129.09, 129.16, 131.01, 133.49, 140,23, 140.35, (aromatic C), 144.21 (N=$\underline{CH}$), 163.0 (im C=N), 173.0 (C=O). Anal. Calc. $C_{22}H_{16}Cl_2N_4O$ (423.29): C, 62.42; H, 3.81; N, 13.24. Found: C, 62.67; H, 3.89; N, 13.59 %.

[2-(4-Nitrobenzylidene)hydrazinyl]-4,4-diphenyl-1*H*-imidazol-5(4*H*)-one (3f)

White powder (70 %),12 h, MP. >300°C decomp., (Lit. 238–240°C) [26]. IR ν cm^{-1}: 3405, 3215 (2NH), 1742 (CO). ^{1}H-NMR, δ ppm: 7.35 – 7.42 (m, 10H, diphenyl), 8.15 – 8.39 (2H, d, J ~ 8 Hz, benzylidene H2,6; 2H, d, J ~ 8 Hz, benzylidene H3,5; 1H, s, N=CH), 9.64 (s,1H, -HN-N=, D_2O exchange), 11.91 (s, 1H, im-NH, D_2O exchange). ^{13}C-NMR, δ ppm: 71.19 (im-C-4), 121.36, 121.59, 123.84, 126.63, 127.10, 127.89, 127.99, 128.33, 128.48, 129.80, 133.54, 133.64, 136.90, 140,16, 140.41, 146.01, (aromatic C), 148.29 (N=$\underline{CH}$), 158.0 (im C=N). Anal. Calcd. for $C_{22}H_{17}N_5O_3$ (399.40): C, 66.16; H, 4.29; N, 17.53; Found: C, 66.38; H, 4.21; N, 17.80 %.

[2-(3-Nitrobenzylidene)hydrazinyl]-4,4-diphenyl-1*H*-imidazol-5(4*H*)-one (3g)

White powder (85 %), 6 h, MP. >300°C decomp. IR ν cm^{-1}: 3405, 3215 (2NH), 1742 (CO). ^{1}H-NMR, δ ppm: 7.34 – 7.42 (m, 10H, Ar–H), 7.65 – 7.73 (m, 1H, benzylidene H-5), 8.21 – 8.23 (m, 1H, Benzylidene H-4), 8.31 – 8.37 (m, 2H, benzylidene H-2,6), 8.69 (s, 1H, N=CH), 9.61 (s,1H, -HN-N=, D_2O exchange), 11.94 (bs, 1H, im-H, D_2O exchange). ^{13}C-NMR, δ ppm: 71.21 (im-C-4), 121.32, 121.60, 123.22, 123.86, 126.65, 127.11, 127.90, 128.00, 128.35, 128.50, 129.82, 129.98,

133.56, 133.64, 136.91, 137.69, 140.17, 140.42, 148.04 (aromatic C), 148.21 (N=$\underline{CH}$), 157.23 (im C=N), 178.0 (C=O). Anal. Calcd. for $C_{22}H_{17}N_5O_3$ (399.40): C, 66.16; H, 4.29; N, 17.53. Found: C, 66.37; H, 4.44; N, 17.81 %.

2-(4-(Dimethylamino)benzylidene) hydrazinyl]-4,4-diphenyl-1*H*-imidazol-5(4*H*)-one (3h)

White powder (81 %), 20 h, MP. 280°C. IR ν cm^{-1}: 3225, 3210 (2NH), 1745 (CO). ^{1}H-NMR, δ ppm: 2.95, 2.97 (2s, 6H, -N(CH$_3$)$_2$), 6.71 (d, J~8 Hz, 2H benzylidene H3,5), 7.29 – 7.42 (m, 10H, diphenyl), 7.66 (d, J ~ 8 Hz, 2H benzylidene H2,6), 8.06 (s, 1H, N=CH), 9.49 (s,1H, -HN-N=, D_2O exchange), 11.72 (bs, 1H, im-NH, D_2O exchange). ^{13}C-NMR, δ ppm: 59.76 (-N(CH$_3$)$_2$, 72.04 (im-C-4), 11.43, 11.62, 120.50, 122.60, 122.69, 124.13, 126.57, 126.72, 127.43, 127.49, 128.10, 128.37, 128.51, 130.97, 137.02, 140.82 (aromatic C-atoms), 145.00 (N=$\underline{CH}$), 160.00 (im $\underline{C}$=N), 172.02 (C=O). Anal. Calcd. For $C_{24}H_{23}N_5O$ (397.47): C, 72.52; H, 5.83; N, 17.62. Found: C, 72.13; H, 6.12; N, 17.65 %.

[2-(2-Hydroxybenzylidene)hydrazinyl]-4,4-diphenyl-1*H*-imidazol-5(4*H*)-one (3i)

White powder (94 %), 6 h, MP. 285°C, (Lit. 216–218°C, Dioxane) [26]. IR ν cm^{-1}: br 3200, 3166 (2NH and OH), 1755 (CO). ^{1}H-NMR, δ ppm: 6.86 – 6.91 (m,2H, benzylidene H-3,5), 7.22 – 7.41 (m,11H, diphenyl and benzylidene H-4), 7.62 – 7.77 (dd, J ~ 8/3 Hz, 1H, benzylidene H-6), 8.47 (s, 1H, N=CH), 9.58 (s,1H, -HN-N=, D_2O exchange), 10.2 (s, 1H, OH, D_2O exchange), 11.72(bs, 1H, im-NH, D_2O exchange). ^{13}C-NMR, δ ppm: 71.40 (im-C-4), 119.04, 119.64, 126.66, 127.13, 127.77, 128.24, 128.45, 129.09, 131.07, 140.41, 144.99 (aromatic C-atoms), 148.0 (N=$\underline{CH}$), 156.75 (im $\underline{C}$=N), 168.0 (C=O). Anal. Calcd. for $C_{22}H_{18}N_4O_2$(370.41) C,71.34; H, 4.90; N, 15.13. Found: C, 71.61; H, 4.79; N,15.32 %.

[2-(4-Hydroxy-3-methoxybenzylidene) hydrazinyl]-4,4-diphenyl-1*H*-imidazol-5(4*H*)-one (3j)

White powder (81 %), 6 h, MP. > 300 °C decomp., (Lit. 260–262°C, Dioxane) [26]. IR ν cm^{-1}: br 3250, 3167 (2NH and OH), 1747 (CO). ^{1}H-NMR(DMSO-d$_6$) δ ppm: 3.83 (s, 3H, OCH$_3$),

6.81 (d,1H, J = 8 Hz, benzylidene H-5), 7.26 – 7.44 (m, 12 H, diphenyl and benzylidene H-2,6), 8.12 (2s, 1H, N=CH), 9.43 (s,1H, -HN-N=, D_2O exchange), 11.34 (s, 2H, im-NH, benzylidene OH D_2O exchange). ^{13}C-NMR δ ppm: 55.95 (OCH$_3$), 71.65 (im. C-4), 111.02, 114.97, 115.45, 121.80, 125.87, 126.68, 127.21, 127.66, 127.88, 128.21, 128.43, 140.60, 140.82, 140.83 (aromatic C-atom), 147.83 (N=CH), 148.88 (im C=N). Anal. Calcd. for $C_{23}H_{20}N_4O_3$ (400.15) C, 68.99; H, 5.03; N, 13.99. Found: C, 69.13; H, 4.87; N,14.04 %.

[2-(2,6-Dimethoxybenzylidene)hydrazinyl]-4,4-diphenyl-1*H*-imidazol-5(4*H*)-one (3k)

White powder (65 %), 6 h; MP. 270–2°C (EtOH/Dioxane). IR ν cm^{-1}: br 3250, 3167 (2NH), 1747 (CO).^{1}H-NMR, δ ppm: 3.78 (s, 6H, 2OCH$_3$), 6.70 (d, J ~ 8 Hz, 2H, benzylidene H-3,5), 7.28 – 7.40 (m, 11H, diphenyl and benzylidene H-4), 8.30 (s, 1H, N=CH), 9.30 (s,1H, -HN-N=, D_2O exchange), 11.82 (s, 1H, im. NH, D_2O exchange). ^{13}C-NMR, δ ppm: 55.95(OCH$_3$), 71.93 (im. C-4), 104.19, 111.12, 126.66, 127.13, 127.44, 128.06, 128.38, 131.17, 140.79, (aromatic C), 144.13 (N=CH), 158.60 (im. C=N), 175.00 (im. C=O). Anal. Calcd. For $C_{24}H_{22}N_4O_3$(414.46) C, 69.55; H, 5.35; N, 13.52. Found: C, 69.25; H, 5.23; N, 13.80 %.

[2-(Furan-2-ylmethylene)hydrazinyl]-4,4-diphenyl-1*H*-imidazol-5(4*H*)-one (3l)

White powder (76 %), 6 h, MP. 288-90°C (EtOH/Dioxane). IR ν cm-1: 3429, 3228 (2NH), 1700 (CO). ^{1}H-NMR, δ ppm: 6.62 (d, J ~ 12, 1H, furan-H-4), 6.93 (d, J ~ 4Hz, 1H, furan H-3), 7.34 (m, 10H, diphenyl), 7.76 (d, J ~12 Hz, 1H, furan H-5), 8.10 (s, 1H, -N=CH), 9.43 (s, 1H, -HN-N=,D_2O exchange), 11.66 (s, 1H, im-NH, D_2O exchange). ^{13}C-NMR, δ ppm: 71.58 (Im. C-4), 112.28, 113.06, 126.72, 127.19, 127.78, 128.26, 128.54, 139.64, 140.55 (aromatic C-atoms), 144.83 (N=CH), 150.03 (im. C=N). Anal. Calcd. for $C_{20}H_{16}N_4O_2$ (.344.37) C, 69.76; H, 4.68; N, 16.27. Found: C, 69.85; H, 4.82; N, 16.39 %.

Synthesis of the arylethylidene hydrazones (4a – h)

A mixture of **2** (2.66 g, 10 mmol) and the appropriate acetophenone derivative (10 mmol) in 20 mL absolute ethanol, containing glacial acetic acid (1 mL), was refluxed till completion as monitored by TLC. The reaction mixture was cooled, the precipitated product was separated by filtration and crystallized from ethanol. Reaction time, %Yield, MP, spectral & elemental data are listed as follows:

Diphenyl-2-(2-(1-phenylethylidene) hydrazinyl)-1*H*-imidazol-5(4*H*)-one (4a)

Yellow crystals (90%), 6 h, MP. 170-2°C (lit. 148 °C. [27]). IR (KBr): ν 3166, 3340 (2NH), 1722 (C=O) cm^{-1}. ^{1}H-NMR, δ 2.34 (s, 3H, CH3), 7.32–7.44 (m, 13H, diphenyl and phenyl H-3,4,5), 8.00 – 8.05 (dd, 2H, J ~ 8/2 Hz, phenyl H-2,6), 9.23 (s, 1H, -HN-N=, D_2O exchange), 11.56 (s, 1H, im-NH, D_2O exchange). ^{13}C-NMR, δ ppm: 21.06 (CH$_3$), 71.13 (im.C-4), 126.85, 126.69, 127.23, 127.81, 128.05, 128.26, 128.44, 128.71, 128.87, 138.44, 138.81, 140.48, and 140.81 (aromatic C-atoms). 154.88 (CH$_3$-<u>C</u>=N), 158.90 (im.C=N), 172.11 (C=O). Anal. Calcd. for C23H20ON4O (368.16): C, 74.98; H, 5.74; N, 15.21%. Found: C, 74.71; H, 5.82; N, 15.37%.

{2-[1-(4-Bromophenyl)ethylidene] hydrazinyl}-4,4-diphenyl-1*H*-imidazol-5(4*H*)-one (4b)

Yellow crystals (70%), 12 h, MP. 194 °C, IR (KBr): ν 3166, 3340 (2NH), 1722 (C=O) cm^{-1}; ^{1}H-NMR, δ ppm: 2.31 (s, 3H, CH3), 7.37–7.41 (m, 10H, diphenyl H), 7.55 – 7.59 (d, J ~ 8Hz, 2H, 4-Br-ph H-3,5), 7.94 – 7.98 (d, J ~ 8Hz, 2H, 4-Br-ph H-2,6), 11.6 (bs, 1H, im-NH, D_2O exchange). ^{13}C-NMR, δ ppm: 18.55 (CH$_3$), 70.90 (im.C-4), 122.24, 123.42, 126.64, 127.17, 127.84, 128.26, 128.42, 128.56, 130.72, 130.88, 131.41, 136.91, 137.69, 140.32, and 140.66(aromatic-C), 154.00 (CH$_3$-<u>C</u>=N), 157.00 (im. C=N), 173.0 (C=O). Anal. Calcd. for $C_{23}H_{19}BrN_4O$ (447.33): C, 61.75; H, 4.28; N, 12.52. Found: C, 61.57; H, 4.46; N, 12.78%

Diphenyl-2-{2-[1-(p-tolyl)ethylidene] hydrazinyl}-1*H*-imidazol-5(4*H*)-one (4c)

Yellow crystals (65%), 20 h; MP. 168 °C. IR (KBr): ν 3166, 3340 (2NH), 1722 (C=O)cm^{-1}; ^{1}H-NMR, δ ppm: 2.32, 2.35 (2s, 6H, 2CH3), 7.18 – 7.44 (m, 12H, diphenyl and p-tolyl H-3,5), 7.80 – 7.93 (d, J ~ 8 Hz, 2H, p-tolyl H-2,6), 9.22 (s, 1H,N-NH, D_2O

exchange), 11.51 (bs, 1H, im-NH, D$_2$O exchange). ^{13}C-NMR, δ ppm: 15.48, 21.42 (2 CH$_3$), 72.06 (im.C-4), 127.44, 127.72, 127.75, 128.75, 129.23, 129.31, 129.43, 129.66, 134.17, 138.19, and 140.86 (aromatic-C), 156.26 (C=N), 159.82 (im. C=N), 175.00 (C=O). Anal. Calcd. for C$_{24}$H$_{22}$N$_4$O (382.46): C, 75.37; H, 5.80; N, 14.65. Found: C, 75.09; H, 5.63; N, 14.91%.

{2-[1-(4-Aminophenyl)ethylidene] hydrazinyl}-4,4-diphenyl-1*H*-imidazol-5(4*H*)-one (4d):

Yellow crystals (80%), 20 h, MP. 194 °C., IR (KBr): ν 3166, 3340 (2NH), 1722 (C=O)cm^{-1}; ^{1}H-NMR, δ ppm: 2.24 (s, 3H, CH3), 5.39 (bs, 2H, NH$_2$,D$_2$O exchange), 6.55 (d, J ~ 8 Hz, 2H, 4-NH$_2$ph H-3,5), 7.32 –7.43 (m, 10H, diphenyl H), 7.73 (d, J ~ 8 Hz, 2H, 4-NH$_2$ph H-2,6), 9.16 (s, 1H, -HN-N=, D$_2$O exchange), 11.60 (bs, 1H, im-NH, D$_2$O exchange). ^{13}C-NMR, δ ppm: 21.53 (CH$_3$), 71.76 (im.C-4), 112.96, 113.54, 126.04, 127.05, 127.18, 127.73, 128.08, 128.24, 128.34, 128.61, 128.63, 141.26, and 150.42 (aromatic-C), 155.17 (CH$_3$-<u>C</u>=N), 160.96 (im. C=N), 172.51 (C=O). Anal. Calcd. for C$_{23}$H$_{21}$N$_5$O (383.45): C, 75.37; H, 5.80; N, 14.65. Found: C, 75.38; H, 5.94; N, 14.88%.

{2-[1-(4-Hydroxyphenyl)ethylidene] hydrazinyl}-4,4-diphenyl-1*H*-imidazol-5(4*H*)-one (4e):

Yellow crystals (98%); 12 h; MP. 211°C. IR (KBr): ν 3166, 3340 (2NH), 1722 (C=O) cm^{-1}; ^{1}H-NMR, δ ppm: δ 1.92 (s, 3H, CH3), 6.80 (d, J ~ 8 Hz, 2H, 4-OH.ph H-3,5), 7.33 – 7.42 (m, 10H, diphenyl), 7.71 (d, J ~ 8 Hz, 2H, H-2,6), 8.09 (s, 1H, OH D$_2$O exchange), 9.49 (s, 1H, -HN-N=, D$_2$O exchange), 11.72 (bs, 1H, im-NH, D$_2$O exchange). ^{13}C-NMR, δ ppm: 21.07 (CH$_3$), 71.62 (im.C-4), 115.42, 125.52, 126.67, 127.14, 127.58, 128.17, 128.41, 129.24, 140.67, and 148.43 (aromatic-C), 159.30 (CH$_3$-<u>C</u>=N), 160.60 (im. C=N), 172.02 (C=O). Anal. Calcd for C$_{23}$H$_{20}$N$_4$O$_2$ (384.43): C, 71.86; H, 5.24; N, 14.57. Found: C, 71.98; H, 5.40; N, 14.31%.

{2-[1-(4-Chlorophenyl)ethylidene] hydrazinyl}-4,4-diphenyl-1*H*-imidazol-5(4*H*)-one (4f)

Yellow crystals (70%); 12 h; MP. 194 °C; IR (KBr): ν 3166, 3340 (2NH), 1722 (C=O), cm^{-1}; ^{1}H-NMR, δ ppm: 2.32 (s, 3H, CH3), 7.36–7.44 (m, 12H, diphenyl and 4Cl-ph H-3,5), 8.06 – 8.09 (d, J ~ 8 Hz, 2H, 4-Cl-ph H-2,6), 9.26 (s, 1H, -HN-N=, D$_2$O exchange), 11.51 (bs, 1H-im. NH, D$_2$O exchange). ^{13}C-NMR, δ ppm: 18.56 (CH$_3$), 71.06 (im.C-4), 127.14, 127.53, 127.66,128.33, 128.46, 128.65, 128.75, 128.91, 133.55, 133.96, 137.63, 138.10, 140.83, 141.17 (aromatic C-atoms), 154.44 (CH$_3$<u>C</u>=N), 161.0 (im <u>C</u>=N), 174.34 (C=O). Anal. Calcd. for: C$_{23}$H$_{19}$ClN$_4$O (402.88): C, 68.57; H, 4.75; N, 13.91. Found: C, 68.87; H, 4.88; N, 14.17%.

{2-[1-(4-Methoxyphenyl)ethylidene] hydrazinyl}-4,4-diphenyl-1*H*-imidazol-5(4*H*)-one (4g):

Yellow crystals (65%); 20 h; MP. 168°C. IR (KBr): ν 3166, 3340 (2NH), 1722 (C=O) cm^{-1}; ^{1}H-NMR, δ ppm: 2.31 (s, 3H, CH3), 3.78 (s, 3H, -OCH$_3$), 6.91–6.94 (d, J ~ 8 Hz, 2H, p-methoxyphenyl H-3,5), 7.32–7.44 (m, 10H, diphenyl H), 7.97–7.99 (d, J ~ 8 Hz, 2H, 4-OCH$_3$-phenyl H-2,6), 9.20 (s, 1H, -HN-N=, D$_2$O exchange), 11.29 (bs, 1H, im-NH, D$_2$O exchange). ^{13}C-NMR, δ ppm: δ 18.56 (CH$_3$), 55.16 (OCH$_3$), 71.06 (im.C-4), 113.20, 113.38, 126.67, 127.21, 127.72, 127.83, 127.89, 128.08, 128.21, 128.40, 130.90, 131.45, 140.58, 140,89, and (aromatic-C), 154.62(CH3<u>C</u>=N), 160.01(im-C=N), 173.78 (C=O). Anal. Calcd for C$_{24}$H$_{22}$N4O$_2$ (398.46): C, 72.34; H, 5.57; N, 14.06. Found: C, 72.50; H, 5.72; N, 14.25%.

4-Diphenyl-2-{2-[1-(thiophen-2-yl)ethylidene]hydrazinyl}-1*H*-imidazol-5(4*H*)-one (4h):

Yellow crystals (65%); 20 h; MP. 168 °C. IR (KBr): ν3166, 3340 (2NH), 1722 (C=O)cm^{-1}.^{1}H-NMR, δ ppm: δ 2.34 (s, 3H, CH3), 7.07–7.08 (ddd, J ~ 8/4/4Hz,1H, thienyl H-4), 7.32–7.35(m, 12H, diphenyl H and thienyl H-3,5), 8.91 (s, 1H, -HN-N=, D$_2$O exchange), 11.35 (bs, 1H, im-NH, D$_2$O exchange) ^{13}C-NMR, δ ppm: 19.0 (CH$_3$), 70.93 (im.C-4), 126.11, 126.67, 127.28, 127.40, 127.66, 127.85, 128.07, 128.24, 128.43,

140.35, 140.74, 144.25 (aromatic-C), 151.92 (CH$_3$-$\underline{C}$=N), 158.90 (im. C=N), 172.11 (C=O). Anal. Calcd. for C$_{21}$H$_{18}$N$_4$OS (374.46): C, 67.36; H, 4.85; N, 14.96. Found: C, 67.60; H, 5.13; N, 14.62%.

Synthesis of Isatin hydrazones:

A mixture of **2** (2.66 g, 10 mmol) and the appropriate isatin derivative (10 mmol) in 20 mL absolute ethanol was refluxed till completion as monitored by TLC., in presence of glacial acetic acid (1 mL). The product obtained after cooling was crystallized from absolute ethanol.

[2-(5-Oxo-4,4-Diphenyl-4,5-dihydro-1*H*-imidazol-2-yl)hydrazono]indolin-2-one (5a):

Yellow crystals (85%); 20 h; Yield; MP. > 300 °C. IR vcm^{-1}: br 3250, 3167 (3NH), 1747 (CO). ^{1}H-NMR, δ ppm: 6.84–6.86 (d, J ~ 8Hz, 1H, isat.H-4/7), 6.95–6.99 (d, J ~ 8Hz, 1H, isat.H-5/6), 7.25– 7.29 (d, J ~ 8Hz, 1H, isat.H-6/5), 7.29 –7.42 (m, 10H, diphenyl H), 8.38–8.40 (d, J ~ 8 Hz, 1H, isat. H-7/4), 10.12 (s, 1H, -HN-N=, D$_2$O exchange), 10.51 (s, 1H, isat-NH, D$_2$O exchange), 11.90(bs, 1H, im-NH, D$_2$O exchange). ^{13}C-NMR, δ ppm: 71.40 (im.C-4), 109.98, 117.81, 121.57, 126.61, 127.02, 128.00, 128.22, 128.53, 128.82, 130.91, 139.64, 142.72 (aromatic-C),160.1(im-C=N), 165.97 (Isat. C=O), 174.38 (Im. C=O). Anal. Calcd. for C$_{23}$H$_{17}$N$_5$O$_2$ (395.41), C, 69.86; H, 4.33; N, 17.71. Found: C, 69.98; H, 4.35; N, 17.95%.

Bromo-3-(2-(5-oxo-4,4-diphenyl-4,5-dihydro-1*H*-imidazol-2-yl)hydrazono)indolin-2-one (5b)

Yellow crystals (90%); 20 h; MP. > 300 °C.IR ν: br 3250, 3167 (3NH), 1747 (CO)cm^{-1}. ^{1}H-NMR, δ ppm: 6.84(m, 1H, isat.H-7), 7.42(m, 11H, diphenyl H and isat. H-4), 8.59 (m, 1H, isat. H-6), 10.31 (s, 1H, -HN-N=, D$_2$O exchange), 10.66(s, 1H, isat-NH, D$_2$O exchange), 12.12(bs, 1H, im-NH, D$_2$O exchange). ^{13}C-NMR, δ ppm: 71.62(im.C-4), 111.75, 113.16, 119.36, 126.72, 127.13, 128.24, 128.43, 129.43, 133.00, 139.31, 141.67, 142.50, (aromatic-C), 160.63 (im-C=N), 165.30 (isat-C=O), 174.12 (im C=O). Anal. Calcd. for C$_{23}$H$_{16}$BrN$_5$O$_2$ (474.31), C, 58.24; H, 3.40; N, 14.77. Found: C, 58.47; H, 3.59; N, 14.38%.

Biology
Antibacterial screening
Bacterial strains and culture conditions

M. smegmatis strain ATCC607^{TM} (Microbiologics®, France) was used to test the antimycobacterial activity of the synthesized compounds. The bacterium was cultured in Middlebrook 7H9 broth (Difco, USA) supplemented with 10 % oleic acid-albumin-dextrose-catalase enrichment (OADC, Becton, Dickinson and Company, USA), 0.5 % glycerol (Sigma, USA) and 0.02 % Tween 80 (Sigma, USA), under shaking conditions (100 rpm) at 37 °C for 3 days. 20 % glycerol stocks of bacterial suspension were stored at - 80 °C. When required, bacteria from glycerol stocks were cultured on Middlebrook 7H10 agar (Difco), supplemented with 10 % OADC and 0.5 % glycerol for 3 days at 37 °C.

Susceptibility testing

Preliminary screening of the antimycobacterial activity of the synthesized compounds was performed by the agar well diffusion method [31]. Fresh *M. smegmatis* culture grown on Middlebrook 7H9 broth for 3 days was used to streak the surface of Middlebrook 7H10 agar plates and 6-mm wells were punched into the agar. A 100 *μl* of stock solution (1 mg/ml) of each compound dissolved in dimethyl sulfoxide (DMSO), were then loaded into the wells, and allowed to diffuse into the agar. Isoniazid (INH) was used as a reference drug (positive control) and DMSO as a negative control of the assay. The plates were incubated at 37 °C for 3 days. Zones of growth inhibition (if any) were then measured.

Determination of the Minimal Inhibitory Concentrations

Susceptibility in terms of Minimal Inhibitory Concentration (MIC) was determined by broth microdilution method using 96-well plates according to the guidelines of Clinical and Laboratory Standards Institute [35]. Briefly, fresh culture of *M. smegmatis* was diluted in Middlebrook 7H9 broth to achieve a cell density of about 1x10^6 CFU/ml. A 100 *μl* volume of bacterial suspension was then added to each well. Bacterial cultures. The studied compounds as well as INH were dissolved in DMSO (a final concentration of 1 *mg/ml*). This concentration was used as the stock solution

for all studies. The wells were treated with serial dilutions of

inhibitors in aerobic conditions and incubated at 37 °C for 3 days. Wells containing 200-µl of uninoculated 7H9 broth or untreated bacterial culture served as negative and positive controls, respectively. The MIC was read as a minimal concentration that prevents visible bacterial growth.

Time-kill assay

A fresh 3-day culture of *M. smegmatis* grown in Middlebrook 7H9 broth was diluted to a cell density of approximately 1×10^6 CFU/ml in 10 ml of 7H9 broth containing 2x MIC or 4x MIC of each tested compound. Untreated culture served as a positive control and uninoculated 7H9 medium served as negative control of the assay. Cultures were then incubated at 37 ºC under shaking conditions at 100 rpm. Aliquots were taken at 0, 24, 48, and 72 h, post incubation to enumerate viable bacterial cells. Samples of 20 µl were taken from each culture, serially diluted 10-fold with 180 µl of sterile phosphate buffered saline (PBS) and were plated on Middlebrook 7H10 agar. Plates were incubated at 37 ºC for 3 days and the CFU values were then determined. The assay was conducted in triplicate and the combined data were presented as means of bacterial counts (Log CFU/ml) at each time point. The lower limit of bacterial detection was 100 CFU/ml.

Cytotoxicity determination

The cytotoxic screening was conducted by Cell Culture unit Laboratory, Faculty of Pharmacy, October 6 University, Giza, Egypt. In flat bottom 96 well-microplates, Vero cells (normal kidney epithelial cells derived from an African green monkey) (0.5×105) were cultured in 180 µl/well RPMI media supplemented with 10% fetal bovine serum, 2 µmol/ml L-glutamine, 250 ng/ml fungizone, 100 units/ml penicillin streptomycin solutions at 37°C in a CO_2 incubator. The plates were incubated for 48 h at 37°C in a humidified 5% CO_2 atmosphere to allow cells to settle down. After incubation, the media were removed, and 180 µl/well fresh serum free medium were added to each well. Cells are then treated with 20 µl of different concentrations (500 – 15.62 µM) of the tested compounds. The plates were

then incubated for 48 h at 37°C in a humidified 5% CO_2 atmosphere. After incubation, the media were removed and MTT solution 40 µl/well was added and incubated for additional 4 h. MTT crystals were solubilized by adding acidified isopropanol (160 µl/well) and the plate was shaken at room temperature. This was followed by spectrophotometric determination of the absorbance at 570 nm using the microplate ELISA reader (FLUOstar Omega, BMG, Labtech, Germany). The absorbance of the resulting color is directly proportional to the number of viable cells in each sample. The percentage of relative viability was calculated using the following equation: [Absorbance of treated cells/ Absorbance of control cells)] X 100.

Bioactivity profiling and molecular modeling
Molecular similarity assessment

Shape-based similarity testing was done using ChemMine tools similarity workbench [58]. Compounds were fed as smiles formulas and atom pair (AP) Tanimoto coefficients were automatically generated.

Generation of the pharmacophore model

The structure of the training set compounds (**4a,c,e-g and 5a,b**), were drawn using the Builder module of the MOE version 2020. 102 program and subjected to energy minimization using MMFF94X force. The pharmacophore model was then generated using the Pharmacophore Elucidation module. It was then established by mapping the test set molecules (**B-H**) using the Pharmacophore Search platform and the conformer having the lowest RMSD value was selected.

Inverse docking study

Computer-assisted simulated inverse docking experiment was conducted using Molecular Operating Environment (MOE 2016. 102) software. The docking study involves docking validation step and the testing of four active compounds (**4a,c,e** and **5a**) against the assigned *Mtb* target proteins. The detailed application involves the following steps:

The 3D crystal structures for InhA (PDB ID: **4TZK**), pantothenate synthetase (PDB ID: **3IVX**), FabH (PDB ID: **1U6S**), and cytochrome CYP121A1 (PDB ID: **6GEQ**)

were downloaded from the Protein Data Bank website. Redundant chains, water molecules and any surfactants were discarded. The standard procedure for target preparation was implemented. The co-crystallized ligands were extracted from their corresponding proteins and used as reference molecules for the validation study. The studied compounds were constructed using the Builder module of MOE, collected in a database, and prepared by adding hydrogen, calculating partial charges and energy minimizing using Force Field MMFF94x.

Docking of the studied compounds in the respective active sites using the MOE-Dock, and resulted databases were analyzed for the energy score between the ligands conformers and the enzyme binding sites in kcal/mol. All receptor-ligand complexes were further investigated to examine the binding interactions to select the best docked pose. The best docked complex assumed to represent the protein-ligand interactions, was selected based on docking score, the orientation of the ligands at the active site in a similar manner to reference ligands and preservation of the key interactions.

Molecular docking into Enoyl ACP reductase active site

Molecular modeling studies were carried out at the department of Medicinal Chemistry, Faculty of Pharmacy, Assiut University, Assiut, Egypt. All molecular modeling studies were carried out using Molecular Operating Environment (MOE 2020.102), Chemical Computing Group, Canada) as the computational software. The target compounds were built using the builder interface of the MOE software and subjected to energy minimization until a RMSD gradient of 0.01 Kcal/mol and RMS distance of 0.1 Å with MMFF94X force-field and the partial charges were automatically calculated. The obtained database was then saved as MDB file to be used for docking calculations. X-ray crystal structure of InhA reductase complexed with NAD$^+$/N-cyyclohexyl-4-phenylpyrrolidone-2-carboxamide (PDB entry: **4TZK**) was obtained from the protein data bank, PDB (www.rscb.org). The vicinity of the co-crystallized ligand was specified to be the docking site. London dG was used as the

scoring function. The higher the absolute value of dG, the better the binding affinity between the ligand and the target. The saved pose for the ligand-target complex of each compound was subjected to detailed 2D and 3D analysis for its interactions with the target.

REFERENCES

1. B. Saifullah, M. Z. B. Hussein, and S.H.H. Al Ali, "Controlled-release approaches towards the chemotherapy of tuberculosis", *Int J Nanomedicine*, 7, 5451-5463 (2012).

2. P. Kamsri, C. Hanwarinroj, N. Phusi, T. Pornprom, *et al.,* "Discovery of New and Potent InhA Inhibitors as Antituberculosis Agents: Structure Based Virtual Screening Validated by Biological Assays and X-ray Crystallography", *J Chem Inform Model*, 60(1), 226 – 234 (2020).

3. D.T. Hoagland, J. Liu, and R. B. Lee, "New agents for the treatment of drug-resistant Mycobacterium tuberculosis", *Adv Drug DelivRev*, 102, 55–72 (2016).

4. A. Chollet, L. Maveyraud, C. Lherbet and V. Bernardes-Genisson, "An overview on crystal structures of InhA protein: apo-form, in complex with its natural ligands and inhibitors", *Eur J Med Chem*, 146, 318–343 (2018).

5. B. Phetsuksiri, M. Jackson, H. Scherman, *et al.,* "Unique mechanism of action of the thiourea drug isoxyl on mycobacterium tuberculosis", *J of Biol Chem*, 278(52), 53123-53130 (2003).

6. E.K. Schroeder, O.N. de Souza, D.S. Santos, J.S. Blanchard, and L.A. Basso, "Drugs that inhibit mycolic acid biosynthesis in Mycobacterium tuberculosis", *Curr Pharm Biotechnol*, 3(3), 197–225 (2002).

7. C.E. Barry, D.C. Crick, and M.R. McNeil, "Targeting the formation of the cell wall core of Mycobacterium tuberculosis", *Infect Disord Drug Targets*, 7(2), 182–202 (2007).

8. A. Alahari, X. Trivelli, Y. Guérarde, L. G. Dover, G. S Besra, J. C. Sacchettini, R. C. Reynolds, G. D. Coxon, and L. Kremer, "Thiacetazone, an antitubercular drug that

inhibits cyclopropanation of cell wall mycolic acids in mycobacteria", *PLoS ONE,* 2(12), e1343 (2007).

9. A.S. Xavier, and M. Lakshmanan, "Delamanid: A new armor in combating drug-resistant tuberculosis", *J Pharmacol Pharmacother,* 5(3), 222-224 (2014).

10. M.V. Worley, and S.J Estrada, "Bedaquiline: A Novel Antitubercular Agent for the Treatment of Multidrug-Resistant Tuberculosis", *Pharmacotherapy,* 34(11), 1187–1197 (2014).

11. N. D. Franz, J. M. Belardinelli, M. A. Kaminski, L. C. Dunn, *et al.,* "Design, synthesis, and evaluation of indole-2-Carboxamides with pan anti-mycobacterial activity", *Bioorg Med Chem,* 25(14), 3746–3755 (2017).

12. A. P. Kozikowski, O. K. Onajole, J. Stec, C. Dupont, A. Viljoen, M. Richard, *et. al.* "Targeting mycolic acid transport by Indole-2-carboxamides for the treatment of M. abscessus infections", *J Med Chem,* 60(13), 5876–5888 (2017).

13. J.S. Freundlich, F. Wang, C. Vilcheze, *et al.,* "Triclosan derivatives: towards potent inhibitors of drug-sensitive and drug-resistant Mycobacterium tuberculosis", *ChemMedChem,* 4(2), 241-248 (2009).

14. X. He, A. Alian, R. Stroud, P.R. Ortiz de Montellano, "Pyrrolidine carboxamides as a novel class of inhibitors of enoyl acyl carrier protein reductase from Mycobacterium tuberculosis", *J Med Chem,* 49(21), 6308-6323 (2006).

15. M. Boff de Ávila, G. Bitencourt-Ferreira, and W.F. de Azevedo, "Structural Basis for inhibition of Enoyl-[Acyl Carrier Protein] Reductase (InhA) from Mycobacterium tuberculosis", *Curr Med Chem*, 27(5), 745-759 (2020).

16. M. Biava, G. C. Porretta, G. Poce, C. Battilocchio, S. Alfonso, A. de Logu, F. Manetti and M. Botta, "Developing pyrrole-derived antimycobacterial agents: a rational lead optimization approach", *ChemMedChem,* 6(4), 593–598(2011).

17. Li Wei, A. Yazidi, A. N. Pandya, P. Hegde, W. Tong. V, C. N. de Moura, E. J. North, J. Sygusch and M. Jackson, "MmpL3 as a Target for the Treatment of Drug-Resistant Nontuberculous Mycobacterial Infections", *Front Microbiol,* 9, 1547 (2018).

18. M.R.G. Fahmi, and Y.S. Kurniawan, "Heterocyclic hydrazone derivatives as potential antitubercular agent against Mycobacterium tuberculosis", *J Experim Clin Microbiol,* 2(2), 16 -21 (2019).

19. Y. Teneva, R. Simeonova, V. Valcheva, and V.T. Angelova, "Recent Advances in Antituberculosis Drug Discovery Based on Hydrazide–Hydrazone and Thiadiazole Derivatives Targeting InhA", *Pharmaceuticals,* 16(4), 484 (2023).

20. R.M. Beteck, R. Seldon, A. Jordaan, D.F. Warner, H.C. Hoppe, D. Laming, L.J. Legoabe and S.D. Khanye, "Quinolone-isoniazid hybrids: synthesis and preliminary in vitro cytotoxicity and anti-tuberculosis evaluation", *Med Chem Comm,* 10(2), 326-331 (2019).

21. V. Velezheva, P. Brennan, P. Ivanov, A. Kornienko, S. Lyubimov, K. Kazarian, B. Nikonenko, K. Majorov and A. Apt, "Synthesis and antituberculosis activity of indole-pyridine derived hydrazides, hydrazide-hydrazones, and thiosemicarbazones", *Bioorg Med Chem Lett,* 26(3), 978-985 (2016).

22. Ł. Popiołek, "Hydrazide-hydrazones as potential antimicrobial agents: overview of the literature since 2010", *Med Chem Res,* 26(2), 287-301 (2017).

23. P. Kumar, K. Kadyan, M. Duhan, J. Sindhu, V. Singh and B.S. Saharan, "Design, synthesis, conformational and molecular docking study of some novel acyl hydrazone based molecular hybrids as antimalarial and antimicrobial agents", *Chem Cent J,* 11(1), 115 (2017).

24. D. A. Heerding, L. T. Christmann, T. Clark, J. W. Venslavsky, D. J. Holmes, S. F. Rittenhouse and D. T. Takata, "1,4-Disubstituted imidazoles are potential antibacterial agents functioning as inhibitors of enoyl acyl carrier protein reductase (FabI)", *Bioorg Med Chem Lett,* 11, 2061-2065 (2001).

25. G. G. Muccioli, J. H. Poupaert, J. Wouters, B. Norberg, W. Poppitz, K. Gerhard, and D.M Lamberta, "A rapid and efficient microwave-assisted synthesis of

hydantoins and thiohydantoins", *Tetrahedron,* 59(8), 1301-1307 (2003).

26. S.M. Gomha, and H.M.E. Hassaneen, "Synthesis and Antimicrobial Activity of Some New Pyrazoles, Fused Pyrazolo[3,4-d]-pyrimidine and 1,2-Dihydroimidazo-[2,1-c][1,2,4]triazin-6-one Derivatives", *Molecules,* 16(8), 6549 – 6560 (2011).

27. T.A. Farghaly, S.M. Gomha, and M.M. Abdalla, "Synthesis of a new series of angiotensin II receptor antagonists and antibacterial agents", *Arch Pharm Res,* 37, 306-314 (2014).

28. A. Awantu, Y. Fongang, G. Ayimele, E. Nantia, P. Fokou, F. Boyom, C. Ngwang, B. Lenta, and S. Ngouela, "Novel Hydralazine Schiff Base Derivatives and Their Antimicrobial, antioxidant, and Antiplasmodial Properties", *Int J Org Chem*, 10(1), 1-16 (2020).

29. J. Taira, T. Nagano, M. Kitamura, M. Yamaguchi, H. Sakamoto and S. Aoki, "Structural modification of a novel inhibitor for mycobacterium enoyl‑ acyl carrier protein reductase assisted by in silico structure‑ based drug screening", *Int J Microbiol*, 9(1), 12-17 (2020).

30. R. E. Gordon, and M. M. Smith, "Rapidly growing, acid fast bacteria. I. Species' descriptions of Mycobacterium phlei and Mycobacterium smegmatis", *J Bacteriol*, 66(1), 41 – 48 (1953).

31. R. S. Gupta, B. Lo and J. Son, "Phylogenomic and Comparative Genomic Studies Robustly support Division of the Genus Mycobacterium into an Emended genus Mycobacterium and Four Novel Genera", *Front Microbiol*, 9, 67 (2018).

32. A. Mohan, J. Padiadpu, P. Baloni and N. Chandra, "Complete Genome Sequences of *M. smegmatis* Laboratory Strain (MC2 155) and Isoniazid-Resistant (4XR1/R2) Mutant Strains", *Genome Announc*, 3(1), e01520 (2015).

33. N. C. Santos, R. B.de Lima Scodro , E. G. Sampiron, *et al.,* "Minimum Bactericidal Concentration Techniques in Myco-bacterium tuberculosis: A Systematic Review", *Microb Drug Resist* , 26(7), 752-765 (2020).

34. CLSI, "Methods for Determining Bactericidal Activity of Antimicrobial Agents". Approved Guideline, *CLSI document M26-A*. Wayne, PA: Clinical and Laboratory Standards Institute (1998).

35. F. Alshareef, "Protocol to Evaluate Antibacterial Activity MIC, FIC and Time Kill Methods'", *ASMI*, 4(5), 2 – 6 (2021).

36. T. Mosmann, "Rapid colorimetric assay for cellular growth and survival: application to proliferation and cytotoxicity assays", *J Immunol Methods*, 65(1-2), 55 – 63 (1983).

37. I. Orme, "Search for new drugs for treatment of tuberculosis", *Antimicrob Agents Chemother*, 45(7), 1943-1946 (2001).

38. S. L. Kinnings, and R. M. Jackson, "ReverseScreen 3D: a structure-based ligand matching method to identify protein targets*", J Chem Inf Model,* 51(3), 624-634 (2011).

39. X. Liu, S. Ouyang, B. Yu, *et al.,* "PharmMapper server: A web server for potential drug target identification using pharmacophore mapping approach", *Nucleic Acids Res,* 38, W609 - W614 (2010).

40. T.W.H. Backman, Y. Cao, and T. Girke, "ChemMine tools: an online service for analyzing and clustering small molecules", *Nucleic Acids Res,* 39(suppl), W486-W491 (2011).

41. C.M. Dobson, "Chemical space, and biology", *Nature,* 432, 824 - 828 (2004).

42. Xin He, A. Alian, R. Stroud, and P. R. Ortiz de Montellano, "Pyrrolidine Carboxamides as a Novel Class of Inhibitors of Enoyl Acyl Carrier Protein Reductase from Mycobacterium tuberculosis", *J Med Chem,* 49(21), 6308 - 6323 (2006).

43. A. Yadav, C. P. Kaushik, and M. Kumar, "Hydrazones tethered disubstituted 1,2,3-triazoles: Design, synthesis, antitubercular and antimicrobial evaluation", *J of Mol Structure,* 1283, 135163 (2023).

44. V.T., Angelova, T. Pencheva, N. Vassilev, *et al.,* "New indole and indazole derivatives as potential antimycobacterial agents", *Med Chem Research*, 28(4), 485-497 (2019).

45. B. Zhang, Li Jun, X. Yang, L. Wu, *et al.,* "Crystal Structures of Membrane

Transporter MmpL3, an Anti-TB Drug Target", *Cell,* 176(3), 636 – 648 (2019).

46. P. B. Devi, S. Jogula, A. P. Reddy, S. Saxena, J. P. Sridevi, D. Sriram, and P. Yogeeswari, "Design of Novel Mycobacterium tuberculosis Pantothenate Synthetase Inhibitors: Virtual Screening, Synthesis, and In Vitro Biological Activities", *Mol Inform,* 34(2-3), 147-159 (2015).

47. N. W. Hassan, M. N. Saudi, Y. S. Abdel-Ghany, A. Ismail, P. A. Elzahhar, D. Sriram, R. Nassra, M. M. Abdel-Aziz and S. A. El-Hawash, "Novel pyrazine based anti-tubercular agents: Design, synthesis, biological evaluation and in silico studies", *Bioorg Chem*, 96, 103610 (2020).

48. J. Zitko, O. Jand'ourek, P. Paterová, L. Navrátilová, J. Kuneš, J. Vinšová and M. Doležal, "Design, synthesis and antimycobacterial activity of hybrid molecules combining pyrazinamide with a 4-phenylthiazol-2-amine scaffold", *Med Chem Comm*, 9(4), 685 - 696 (2018).

49. S. M. Kishk, K. J. McLean, S. Sood, D. Smith, *et al.,* "Design and Synthesis of Imidazole and Triazole Pyrazoles as M. Tuberculosis CYP121A1 Inhibitors", *Chemistry Open*, 8(7), 995 -1011 (2019).

50. P.S. Kharkar, S. Warrier, and R. S. Gaud, "Reverse docking: a powerful tool for drug repositioning and drug rescue", *Future Med Chem*, 6(3), 333 - 342 (2014).

51. M. Chebaiki, E. Delfourne, R. Tamhaev, *et al.,* "Discovery of new diarylether inhibitors against Mycobacterium tuberculosis targeting the minor portal of InhA", *Eur J Med Chem*, 259, 115646 (2023).

52. S. L. Parikh, G. Xiao, and P. J. Tonge, "Inhibition of InhA, the enoyl reductase from M. tuberculosis, by triclosan and isoniazid", *Biochemistry*, 38(26), 3623-3634(1999).

53. O., Holas, P. Ondrejcek, and M. Dolezal, "Mycobacterium tuberculosis enoyl-acyl carrier protein reductase inhibitors as potential antituberculotics: development in the past decade", *J Enzyme Inhibit and Med Chem*, 30(4), 629-648(2015).

54. C. A. Lipinski, F. Lombardo, B. W. Dominy, and P. J. Feeney, "Experimental and computational approaches to estimate solubility and permeability in drug discovery and development settings**",** *Adv Drug Deliv Rev*, 46(1-3), 3 - 26(2001).

55. D. F. Veber, S. R. Johnson, H. Y. Cheng, B. R. Smith, K. W. Ward, K. D. Kopple, "Molecular properties that influence the oral bioavailability of drug candidates", *J Med Chem,* 45, 2615 – 2623 (2002).

56. A. Jarrahpour, J. Fathi, M. Mimouni, T. Ben Hadda, J. Sheikh, Z. H. Chohan and A. Parvez, "Petra, Osiris and Molinspiration (POM) together as a successful support in drug design: antibacterial activity and biopharmaceutical characterization of some azo Schiff bases", *Med Chem Res,* 21, 1984–1990 (2012).

57. A. Parvez, M. Jyotsna, M. H. Youssoufi and T. Ben Hadda, "Theoretical Calculations and Experimental Verification of the Antibacterial Potential of Some Monocyclic β-Lactams Containing Two Synergetic Buried Antibacterial Pharmacophore Sites", *Phosphorus Sulfur Silicon Relat Elem,* 7, 1500–1510 (2010).

58. ChemMine tools: an online service for analyzing and clustering small molecules. Available at :http://chemmine.ucr.edu/ (Accessed: 15 March 2024)..

نشرة العلوم الصيدليـــة

جامعة أسيوط

BULL. PHARM. SCI.
Assiut Univ.

دراسة تصميم وتشييد وتنميط الفاعلية البيولوجية لمجموعة من هيدرازونات الإيميدازولينون كمضادات محتملة متعددة الأستهداف ضد الدرن

إيناس عبد الحميد طه[1]* – نادية محفوظ[1,2] – فرغلي عمر[2] – ياسر موسى إبراهيم[3] – أحمد مجاهد أبو وردة[3]

[1]قسم الكيمياء، كلية الصيدلة، جامعة ٦ أكتوبر، مدينة ٦ أكتوبر ١٢٥٨٥، الجيزة ، مصر

[2]قسم الكيمياء الدوائية، كلية الصيدلة، جامعة أسيوط، أسيوط ٧١٥٢٦ ، مصر

[3]قسم الأحياء الدقيقة، الشعبة العامة للعلوم الطبية الأساسية، هيئة الدواء المصرية، الجيزة ١٢٦١١، مصر

فى اطار الاهتمام لاستنباط مركبات جديدة ذات فاعلية محتملة ضد جرثومة الدرن تم تصميم وتشييد ثلاث مجموعات من الهيدرازونات المشتقة من ٢-هيدرازينيل-٤,٤-ثنائي فينيل ايميدازولينون (3a-l، 4a-h و 5a,b). وفى هذا الصدد تم التحقق من التركيب البنائى للمكبرات المحضـرة باستخدام الوسائل الطيفية المختلفة بالاضافة الى التحليل الدقيق للعناصر. كما تم تقييم فعاليتها في المختبر ضـد جرثومة Mycobacterium smegmatis (ATCC٦٠٧) بالمقارنــة بعقـار أيزونيازيـد (INH) كـدواء مرجعي. وقد اظهرت النتائج أن عشرة من المركبات التي تم اختبارها لها فاعليــة تثبيطيــة مشـابهة للأيزونيازيد تتمثل فى الحد الأدنى لقيم التركيز المثبط (MIC ٠.٠٤٥- ٠.٠٣٢μM; INH = 0.046 μM =). على وجه التحديد، يعد بارا توليل اىثليدين هيدرازون (4c) و٢- اوكسى اندولين ٣ يليـدين (5a) من أقوى المركبات (MIC = ٠.٠٣٣ μM). وفى دراسة حركية التأثير القاتل للميكروب أظهر المركب (5a) تأثيرًا مميتا مكافئًا للأيزونيازيد حيث لوحظ انخفاض في عدد البكتيريا بمقدار ٩٩.٩٪، عنـد تركيز بقيمة ٤ أضعاف التركيز الادنى المثبط بعد ٧٢ ساعة. وقد تم التحقق من انعدام سمية المركبات الاعلى فاعلية (5a,b; 4a,c,e;) ضد خطوط خلايا فيرو عن الحد الأدنى من السمية في المختبر كمـا يتضح من قيم معامل السمية الانتقائي (SI ~ 40 - > 2000). وفى دراسة النمذجة الجزيئيـة اظهرت تحليل ملفات تنميط النشاط الحيوي باستخدام العديد من التطبيقات الحسابية والعكسـية أن المركبـات المستهدفة تتميز بالفاعلية المحتملة ضد عدد من المستهدفات البيولوجية لميكروب الدرن. وقـد تبين أن إنزيم بروتين ناقل الأسيل (InhA) هو الهدف المحتمل الأكثرمصداقية. وقد تم تأكيد ذلك مـن خلال دراسات الالتحام الجزيئي في الموقع النشط لـ (ACP reductase InhA) عن تفاعل واعد مـع الأحماض الأمينية الثلاثية الحفزية، Tyr158، وLys165، وPhe149 . كمــا اظهــرت دراسـة التقييـم الحسابي للصفات الجزيئية والمضاهاة بالعقاقيرللمركبات نتائج واعدة لهذه لإجراء مزيد من التقييمـات كسلسلة جديدة من العوامل المضادة للدرن.